Kinematic and Dynamic Modeling of Nanostructured Origami

by

Paul Steven Stellman

B.S., Texas A&M University (2004)

Submitted to the Department of Mechanical Engineering
in partial fulfillment of the requirements for the degree of

Master of Science

at the

MASSACHUSETTS INSTITUTE OF TECHNOLOGY

February 2006

Signature of Author .....
Department of Mechanical Engineering
25 January 2006

Certified by .....
George Barbastathis
Associate Professor of Mechanical Engineering
Research Head

Accepted by .....
Lallit Anand
Chairperson, Department Committee on Graduate Students

Kinematic and Dynamic Modeling of Nanostructured Origami

by

Paul Steven Stellman

Submitted to the Department of Mechanical Engineering
on 25 January 2006, in partial fulfillment of the
requirements for the degree of
Master of Science

Abstract

Nanostructured Origami is a manufacturing process that folds nanopatterned thin films into a desired 3D shape. This process extends the properties of 3D design and connectivity found in origami artwork to the bulk fabrication of 3D nanostructures. Our technique is a two-step procedure that first patterns the devices in 2D and then folds the membranes to the final 3D shape along pre-defined creases.

This thesis describes theoretical methods that have been developed to model the actuation of origami devices. The background of origami mathematics and advances in robotics are presented in the context of modeling Nanostructured Origami. Unfolding of single-vertex origami is discussed, and an algorithm is implemented to calculate the unfolding trajectories of several devices. Another contribution of this thesis is the presentation of a methodology for modeling the dynamics of two classes of origami: accordion origamis and single-vertex origamis. The forward dynamics and equilibrium analysis of a useful bridge structure and the corner cube origami are simulated. The response of a model of an experimental actuation technique is well-behaved, and it is shown that the final folded state of these devices is at a stable equilibrium.

Research Head: Prof. George Barbastathis
Title: Associate Professor of Mechanical Engineering

0.1 Foreword

My short tenure as a graduate student has been an amazing time in my life! I have learned many valuable lessons and forged new relationships that I will carry with me for the rest of my life. MIT has offered me an educational experience that has given me a new perspective on life-long learning. The research presented in this thesis has been an exciting pursuit, and I look forward to continuing my work toward a PhD.

There were many people who made significant contributions to this thesis. First and foremost among these people is my advisor, Professor George Barbastathis. His unyielding support for my work was comforting, and his unmatched enthusiasm radiates toward everyone in his presence. The most rewarding moments, however, were those many one-on-one meetings in which we discussed my research at length. Whether I was tired and out of new ideas or working in the wrong direction entirely, the meetings with George always seemed to spark new enthusiasm toward my research.

Special thanks goes to Professor Erik Demaine of MIT as well. His research in origami mathematics is making rapid advances. I appreciate his conversations with George and me regarding the unfolding of single-vertex origamis, and I am privileged to have been his collaborator.

All my colleagues in the 3D Optical Systems Group were essential to my academic success. There are five students in the group working on the Nanostructured Origami project, and I am excited about the progress that we will make in the future. Special thanks to Tilman Buchner, Will Arora, Hyun Jin In, Tony Nichol, and Nader Shaar for the numerous research discussions and for all of your support for our project. I would also like to thank Satoshi Takahashi for helping me with the research of Chapter 3 during a class in 2004.

I would like to thank my mother, Kay Tettleton, for her unwavering support of me and my career. I truly could not have done it without her help. Also, my stepfather, John Tettleton, has always been supportive of my endeavors and has encouraged me to pursue a career and lifestyle with which I will be happy. Thanks also to my father, Steve Stellman, for his confidence in my abilities and his encouragement. Finally, I would like to thank my girlfriend, Laurie Friesenhahn, for the companionship and love we have shared over the past 15 months.

Cambridge, MA

January 2006

Contents

List of Figures

Chapter 1

Introduction

This thesis describes analytical and numerical modeling techniques used to design and characterize the folding of nanopatterned membranes. The process of patterning devices in 2D and folding to a desired 3D shape is referred to as Nanostructured Origami [1]. Fig. 1-1 shows a schematic of several folded devices on a silicon wafer. The surfaces of the segments can be patterned with any number of devices, including optical, electronic, microfluidic, and mechanical structures. The 2D patterning step is accomplished using any of the industrial or research-grade writing methods such as optical lithography, electron beam lithography, and nanoimprinting. The extensive infrastructure of the semiconductor industry allows this step to be included seamlessly with the origami process, while maintaining the highest patterning resolutions available for the devices [2]. To facilitate the folding of the origami membranes, active and passive creases are also patterned during the first step. Active creases are designed to contain the functionality necessary to actuate the folding motion, while passive creases are thinned films that fold in response to actuation at the active creases.

The second step of Nanostructured Origami is to accurately and repeatedly fold the segments to the desired positions. This requires the actuation method to be controllable and compatible with the fabrication technology. Once a model has been developed for the actuation at a crease, it is possible to predict the motion of the origami system mathematically. The actuation procedure can be modeled as an external torque applied to the creases of the origami, and the required torques can be calculated directly from the origami's geometry and material properties. By gaining knowledge of origami geometry and the system dynamics, the actuation sequence

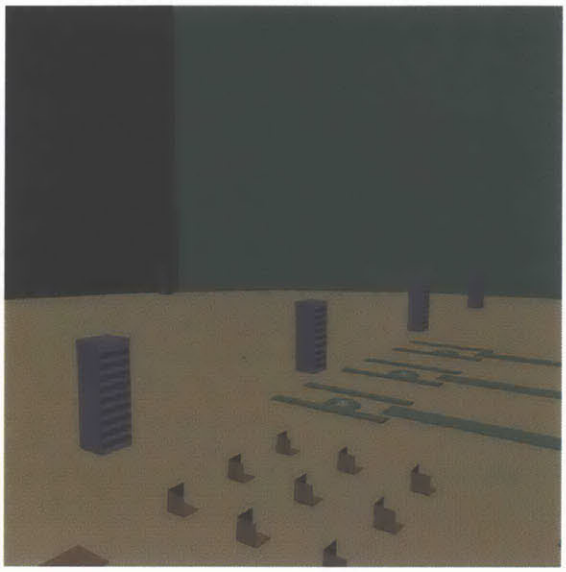

Figure 1-1: Cartoon of folded origamis on a wafer.

can be implemented such that the origami folds correctly to the desired folded state. The concepts introduced in this thesis can also be extended to the case of more complex origamis.

1.1 Inspiration

The inspiration for 3D nanomanufacturing comes from the observation that there is an inherent advantage to using all three geometric dimensions. However, the fabrication of three-dimensional nanostructures is difficult. Current methods are limited largely to either periodic structures fabricated using interferometric lithography or stacked devices formed by multiple sacrificial etches [3]. For non-periodic structures, no other efficient manufacturing method has been developed. The idea for folding patterned thin films arises from both the Japanese art of origami and folding that is observed in nature. Master origamists such as Robert Lang can fold magnificent shapes such as those in Fig. 1-2. Although these shapes are pieces of art with no practical use in nanomanufacturing, the figure illustrates both the high level of connectivity and 3D effectiveness that origami offers. The patterning step in our process gives definition to these surfaces that provides the 3D functionality of Nanostructured Origami.

Consider the schematic of the human brain's cerebral cortex in Fig. 1-3. Washington Uni-

Figure 1-2: Various origami artwork made by Robert Lang. Copyright Robert Lang.

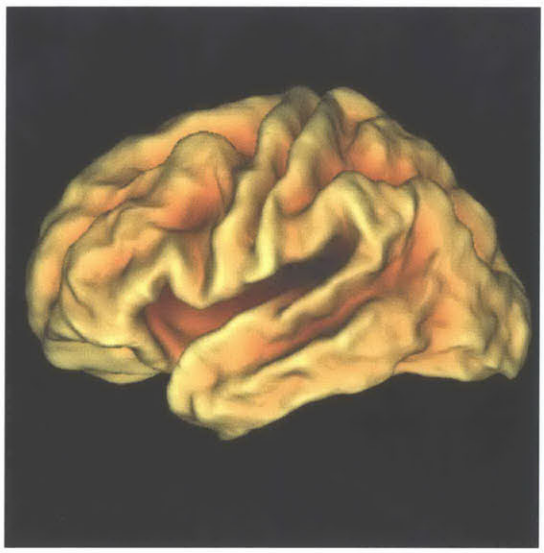

Figure 1-3: 3D surface map of cerebral cortex. Copyright SumsDB 2006.

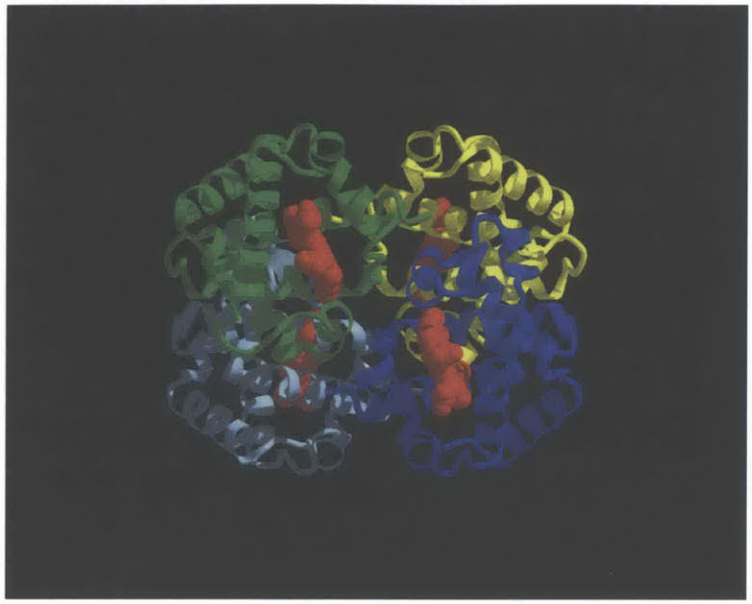

Figure 1-4: 3D model of the protein hemoglobin. Copyright Pittsburgh Supercomputing Center 2006.

versity neuroscientists created this 3D atlas of the folds of the cerebral cortex. Their study maps the folds in the cerebral cortex to brain function. The surface map, called PALS, is a clear example of the 3D functionality that nature has imparted to the brain through folding. These 3D neural connections have high volumetric efficiency and are prime examples of the advantages of 3D interconnections [4].

Another example of the advantages of folding is in the self-assembly of proteins. Proteins are the building blocks of all biological organisms. They consist of a sequence of amino acids that fold themselves into a specific shape. The ultimate goal of the Human Genome Project was to determine the sequence of amino acids for any human protein. This sequence, absent any folding, is simply a one-dimensional string of information that is produced inside the ribosome. The major reason for the protein's functionality, however, is its ability to repeatably and accurately fold to an expected shape. Consider the image in Fig. 1-4 of the protein hemoglobin, which carries oxygen through the bloodstream [5]. This remarkable function is accomplished because its geometry (and the physics associated with its geometry) has been assembled very accurately by forces applied to the chain as it leaves the ribosome.

Analogously, the patterning step in Nanostructured Origami is essentially a two-dimensional surface of information that is written onto a silicon wafer. Electronic, optical, and other types of information are encoded on the wafer surface at very high information density. Similarly, Nanostructured Origami folds a pre-patterned surface into the desired shape. The self-assembly of the origami's folding on a wafer is critical in making complex shapes. Unlike larger 3D man-made structures, such as skyscrapers, the small length scales that define both proteins and nanopatterned origamis necessitate automatic folding processes. Systems such as the Atomic Force Microscope (AFM) can manipulate matter on the atomic scale, but the AFM writes serially and hence is inefficient for bulk fabrication. Just as computational modeling has been essential in understanding the structure of proteins [6],[18], modeling facilitates a deeper understanding of the self-actuation of origami.

1.2 Applications

The previous section described our motivation for pursuing the development of a robust 3D nanomanufacturing technique. Given that Nanostructured Origami is a generic manufacturing process, there is not one specific application that we are trying to employ. Instead, the origami process should be viewed as a platform for making arbitrary shapes. A few example applications include an electrochemical supercapacitor, 3D photonic crystals, negative index materials, a corner cube retroreflector, and a bridge device for optical interconnects. The supercapacitor, photonic crystals, and negative index material will briefly be described in this section, while the corner cube and bridge are analyzed and modeled in Chapter 5.

An electrochemical supercapacitor was created using the Nanostructured Origami technique and is presented in [7]. The device is a type of accordion origami in which an electrode coated in some form of carbon is folded over a fixed electrode. The device can be used as a power source for any number of microelectromechanical systems. Testing indicates that the increased surface area due to folding creates a high capacitance. A schematic of the supercapacitor and scanning electron micrographs of the actual SU-8 device are shown in Fig. 1-5.

Photonic crystals are a class of integrated optical devices that hold great promise in the

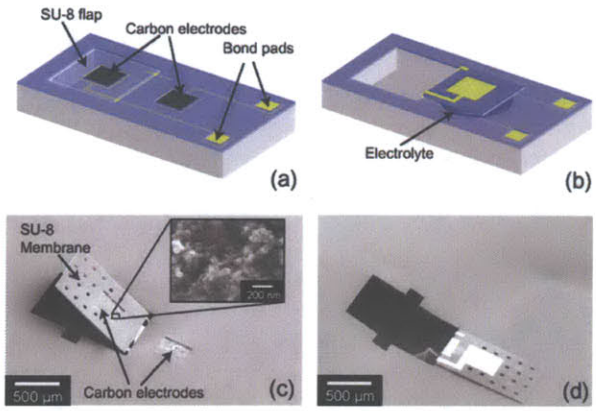

Figure 1-5: Schematic of supercapacitor (a) before folding and (b) after folding. SEM plots of actual device (c) before folding and (d) after folding. Copyright Hyun Jin In 2005.

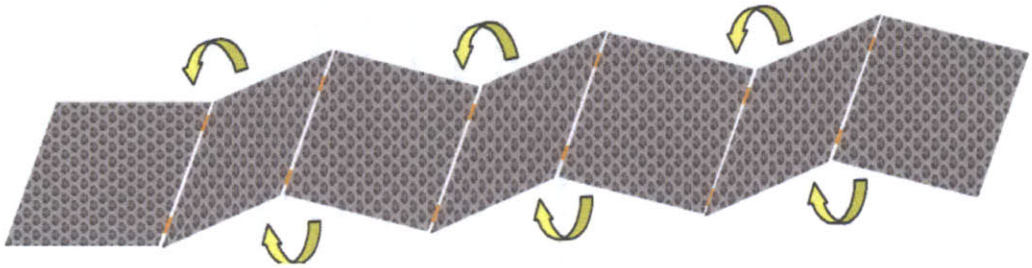

Figure 1-6: Schematic of 3D photonic crystal fabricated using origami.

area of optical computing and communications. Currently, 3D photonic crystals are made by stacking [3]. These devices act as waveguides, and they could potentially be manufactured by folding as an accordion origami. Fig. 1-6 illustrates the accordion concept as applied to a 3D photonic crystal. The major concern when making a photonic crystal is ensuring nanometer-scale alignment. This could potentially be done using nanomagnets or another form of precision alignment technique.

A third application is the fabrication of materials that exhibit a negative index of refraction. Among other applications, these materials can act as "perfect lenses" by amplifying the evanescent optical field. This could potentially beat the diffraction limit for imaging and in the lithography industry. [8] has described a chiral material that exhibits a negative index, which

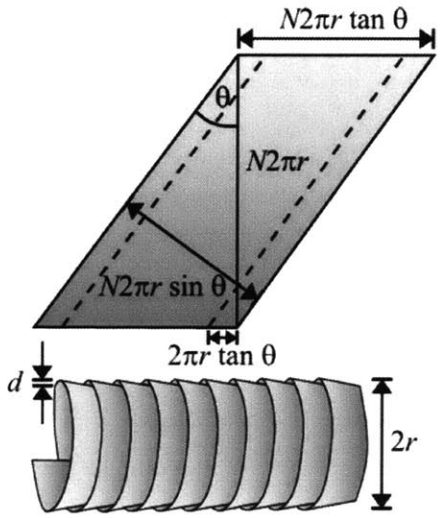

Figure 1-7: Diagram of chiral material proposed as a negative refractive material. Copyright J. Pendry 2004.

is similar to the Swiss roll structures described in [9]. Fig. 1-7 illustrates the design of the chiral material described in [8]. This could be fabricated using a stress actuation method. [10] reports on progress in manufacturing a Swiss roll device using a stress actuation technique, and the chiral material could be fabricated in a very similar manner.

1.3 Actuation Methods

Two experimental actuation mechanisms for Nanostructured Origami are considered in this thesis. In [11], a stress-based actuation procedure is used. For this process, the active hinges consist of a thin film bilayer. A structural layer contains the devices, while a pre-stressed crease bends the structural segments to the desired angle upon release. [11] used silicon nitride as the device layer and chromium as the stressed layer. The folding torque is produced by the stress mismatch between film layers in the origami. The radius of curvature ρ of the bilayer was also predicted accurately in [11] by the relation

$$\rho = \frac{E_1'^2 t_1^4 + E_2'^2 t_2^4 + 2E_1' E_2' t_1 t_2 \left(2t_1^2 + 3t_1 t_2\right)}{6E_1' E_2' t_1 t_2 \left(t_1 + t_2\right)\left(C/E_2'\right)}, \tag{1.1}$$

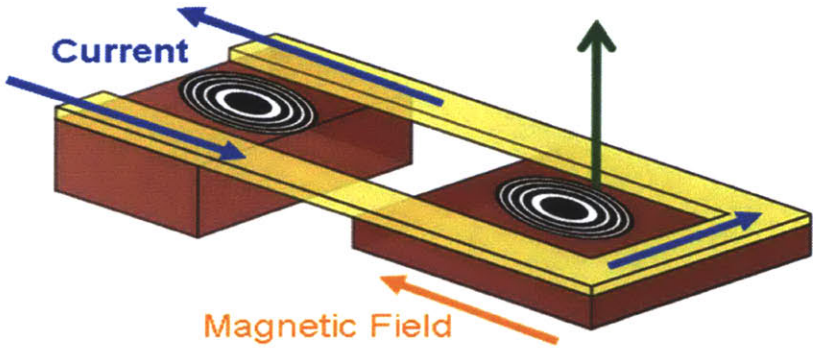

Figure 1-8: Drawing of the Lorentz force actuation procedure.

where the values of the variables are defined in [11]. Chapter 5 describes in detail this actuation technique in the context of the folding of two different origamis.

Another method explored in [1] patterns gold hinges around which the origami folds, while SU-8 contains the devices. To fold the origami, electrical current passes through the gold in the presence of a magnetic field, resulting in a Lorentz force. Fig. 1-8 shows a schematic of the Lorentz force actuation method.

1.4 Overview of the Thesis

This thesis is organized as follows. Chapter 2 presents background research and a review of literature. The review includes work performed by the origami mathematics community as well as a brief review of research accomplishments from the robotics community. Together, this body of knowledge provides a solid basis for the investigation of modeling Nanostructured Origami. Chapter 3 explores the unfolding of single-vertex origamis using energy methods based on previous work by Erik Demaine on unfolding linkages. A general formulation for origami dynamics is defined in Chapter 4, and example implementations of an accordion origami and corner cube are presented in Chapter 5. Chapter 6 concludes the thesis.

Chapter 2

Background

This thesis draws largely from both the origami mathematics community and the robotics community. Origami mathematicians and computational geometricians have made astounding advances in understanding the geometry of origamis in recent years. Despite the significant progress in research on the geometry of origami, little research has been completed in understanding the physics of origami folding. Thus, our work also employs methods developed for modeling the dynamics of articulated robot arms.

2.1 Geometry of Folding and Unfolding

2.1.1 Unfolding Techniques

There has recently been a great deal of work done on the unfolding of linkages. The primary research question is referred to as the Carpenter's Rule problem. The two-dimensional version of Carpenter's Rule states, "Convexify a simple bar-and-joint planar polygonal linkage using only non-self-intersecting planar motions" [12]. Connelly, Demaine, and Rote proved that there are no locked chains in 2D [13]. The physical meaning of this proof is that no two configurations of a chain in two dimensions can be prevented from reaching one another via continuous motions.

The obvious question that arises is whether there is an algorithm that can convexify or straighten an arbitrary 2-D linkage. Prior work [14], [12], [15] has answered this question in the affirmative. In [14], the problem is established as a convex optimization problem. The

unfolding motion of the linkage is modeled by an ordinary differential equation of the form [14]

$$\mathbf{p}'(t) = \mathbf{v}(t), \ \mathbf{p}(0) = \mathbf{p}. \tag{2.1}$$

The initial configuration of the linkage is $\mathbf{p}$, and $\mathbf{v}$ is the solution to a convex optimization problem with constraints. [14] implemented a standard forward Euler technique to solve the differential equation.

Another method of unlocking linkages was developed by [12] and [16] based on pseudo-triangulations. According to [12], a *pseudo-triangle* is a "simple polygon with three vertices on its convex hull, joined by three inward convex polygonal chains". The unfolding method involves creating a pseudo-triangulation of the points which represent the joints of the linkage. It was proven that such a pseudo-triangulation (except for any edges that lie on the convex hull) is a chain that has one degree-of-freedom. The algorithm proceeds to use a force to incrementally unfold the linkage using expansive motions along the single degree-of-freedom. Fig. 2-1 illustrates the use of this algorithm to unfold a chain.

The fastest algorithm found to date for the 2D linkage problem was described in 2004 by [15]. The proposed algorithm assigns a repulsive energy function to a graph of vertices that are parameterized to maintain constant edge lengths. The algorithm then follows the steepest descent of energy until the chain has been convexified or straightened. An algorithm for unfolding single-vertex origamis that is based on this research is presented in Chapter 3. Fig. 2-2 illustrates the unlocking of a 2D chain using the energy method presented in [15].

2.1.2 Origami

Origami refers to the Japanese art of paper folding. [17] and [18] present an excellent description of the history of origami mathematics and a survey of many questions relating to the general problem of folding and unfolding. This chapter describes some of the recent algorithmic results that are applicable to Nanostructured Origami.

[19] showed that any 3D object can be folded from an infinitely large square piece of paper. This is true under the assumptions that the paper has zero thickness and that the folds follow the "zig-zag" pattern described in [19]. Of course, this does not necessarily translate into

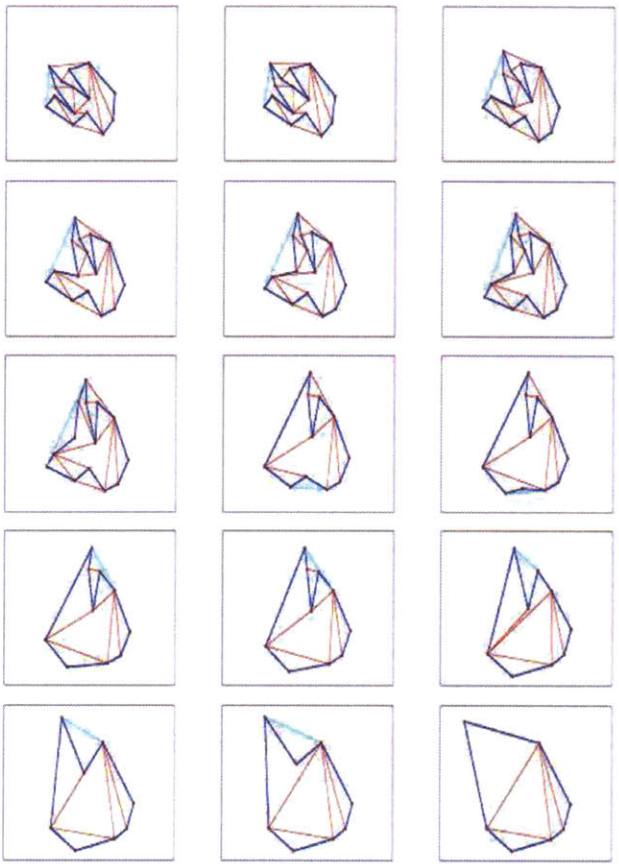

Figure 2-1: The unlocking of 2D linkages using pseudotriangulations. Copyright Ileana Streinu 2004.

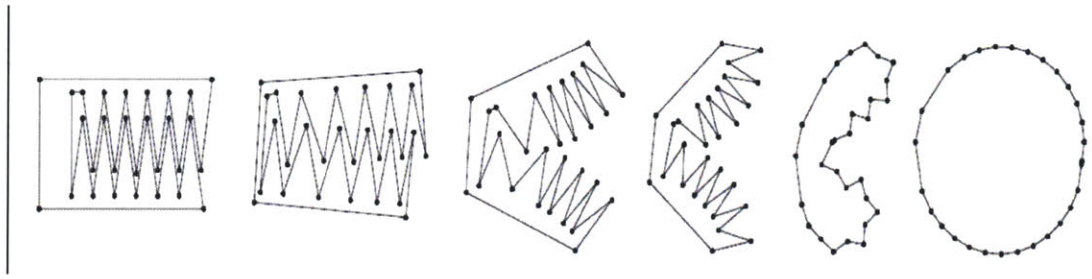

Figure 2-2: Unfolding of 2D chain using energy method. Copyright Cantarella, et al 2004.

the ability to feasibly manufacture an arbitrary origami on a wafer, but it does imply that Nanostructured Origami has the potential to be a very powerful tool in making many complex 3D shapes.

The unfolding question introduced in the previous section of this chapter has been extended to the case of single-vertex origamis by [20]. The proof in [20] shows that every simple, single-vertex origami fold with the fold-vertex interior to the paper, interior to a boundary edge, or situated at a convex vertex can be unfolded with expansive motions. An expansive motion is a motion in which the distances between vertices never decrease. The proof was based on motion of circular arcs along a spherical surface. This result implies that, since expansive motions exist, there should be an algorithm for unfolding along the sphere. Chapter 3 presents research that implements an unfolding algorithm for single-vertex origami using energy methods.

The problem of folding rigid single-vertex origamis was first investigated extensively in [21]. Affine transformations were used to map the folding of the 2D crease pattern to the final 3D shape for single-vertex origamis. The necessary condition for this fold was defined as a multiplication of rotation matrices to form a closed loop. [22] implemented an efficient algorithm to model the kinematics of the corner cube, a rigid single-vertex origami. Through the use of screw calculus [23], [22] determined the kinematic constraint relations for the corner cube and implemented a software tool to visualize its folding. Fig. 2-3 illustrates the corner cube from [22] as it folds.

2.2 Robot Dynamics and Control

The dynamics of robotic manipulators has been extensively studied in the past several years. The modeling techniques that have been used to simulate and control robots have yielded tremendous results in the development of fast and accurate robotic arms. Although the articulated arms are typically viewed as one-dimensional linkages, the mathematical modeling methods can be easily extended to the case of origamis.

Many textbooks are available that describe state-of-the-art mathematical methods for calculating the kinematics and dynamics of robotic manipulators. Excellent texts such as [24] and [25] can be consulted for detailed instruction, and there are many other sources available in the

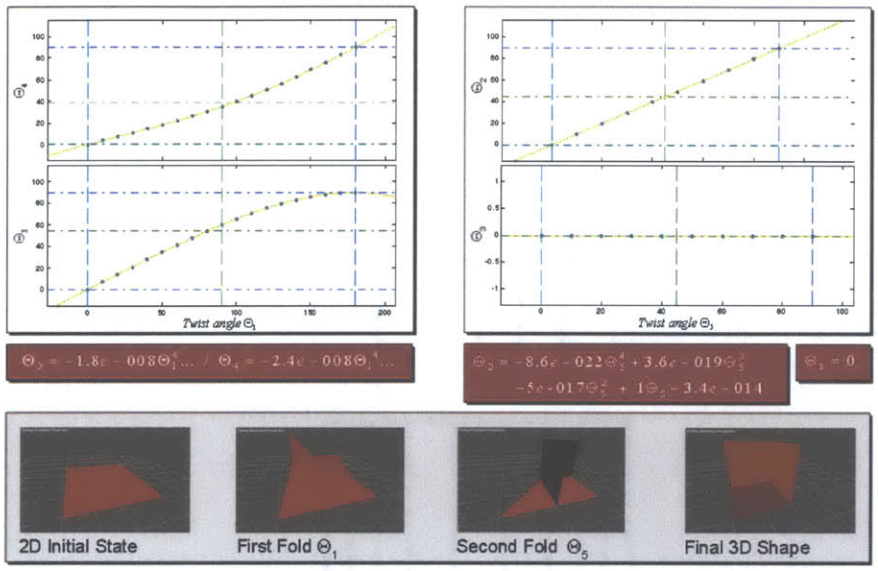

Figure 2-3: Trajectory of corner cube and its kinematic constraints. Copyright Tilman Buchner 2003.

literature. [23] is used extensively as a mathematical background for the results of this thesis. In [23], the treatment of modeling manipulators is based on screw calculus. Chapter 4 provides a mathematical overview of the methods presented in [23].

The general procedure for calculating the input generalized forces for closed loop robotic manipulators was first described by Luh and Zheng based on previous results from Wittenburg. One unactuated crease of the chain is cut to form a reduced system with an open chain topology, and the closed chain torques are calculated in terms of the reduced system torques [26],[27]. Using the principle of virtual work, [28] derived the same relationship as [27] and presented the forward dynamics algorithm as well. In [28]'s approach a velocity constraint matrix was derived directly from the holonomic constraints, while [27] used a Lagrange multiplier formulation. Chapter 4 describes the mathematics for simulating closed chain dynamics using these techniques.

Chapter 3

Unfolding Single-Vertex Origamis

The solution to the origami unfolding problem arguably provides more information about a geometry than does the folding problem. The origami folding problem addresses the questions of what shapes are foldable from a given crease pattern and what trajectory the folding motion follows. There is no unique folding motion for an arbitrary crease pattern, however, because if the actuation is not sequenced properly then there may be collisions. The advantage of unfolding lies in its use of the actual folded shape as an initial condition, eliminating this redundancy. For the purposes of Nanostructured Origami, the folded configuration of a structure is typically known since the device's geometry is dictated by a design's functional requirements.

Besides folding redundancy, solving the unfolding problem also gives information about the "flat unfoldability" of an origami. We define a "flat unfoldable origami" to be an origami which can be unfolded rigidly from its folded state in 3D to the flat state via continuous non-self-intersecting motions. The unfolding problem for origami is analogous to the unfolding of linkages, but the canonical state for origamis is a 2D plane rather than a convex polygon [15]. If the final shape of the origami is not in a plane, then either the origami's integrity condition has been violated by self-intersections or the angle included by the central vertex is less than 360°.

For example, consider the origamis in Fig. 3-1. Fig. 3-1a shows an allowable folding motion that correctly folds the origami to the desired corner cube geometry. Fig. 3-1b also shows an admissible folding of another origami, but the origami is not physically realizable since neither

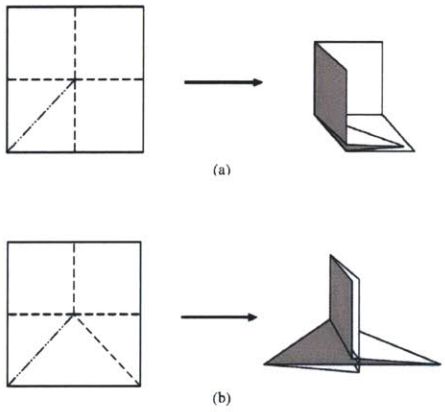

Figure 3-1: (a) Corner cube crease pattern and folded state and (b) Origami fold that is disallowed due to self-intersections

paper nor thin films are allowed to self-intersect [21].

Most origami geometries are overdetermined, introducing dependencies between the joint angles of the origami. Since the unfolding operation maintains the device integrity by enforcing its rigidity, unfolding can be used to determine these constraint relations. By reversing the unfolding path, the method also acts as a path-planning procedure for the forward folding motion. For example, the kinematic constraints of Fig. 2-3 in Chapter 2 are equivalent to the results of this chapter for the corner cube. Although this thesis addresses only single-vertex origamis, both the determination of constraints and path-planning will be essential for the modeling of multiple-vertex origamis. Energy-based modeling techniques such as the method presented here could potentially be used in more complicated models of multiple vertex origamis.

3.1 Energy Methods for Unfolding

Chapter 2 outlined prior literature that describes the unfolding of linkages. The inspiration for using an energy method to model the kinematics of single-vertex origami came from both [15] and research recently reported by Streinu and Whiteley [20].

The model implemented in this thesis uses the mathematical convenience of origami motions along the unit sphere. The idea is to use spherical arcs in the plane of the origami flaps whose

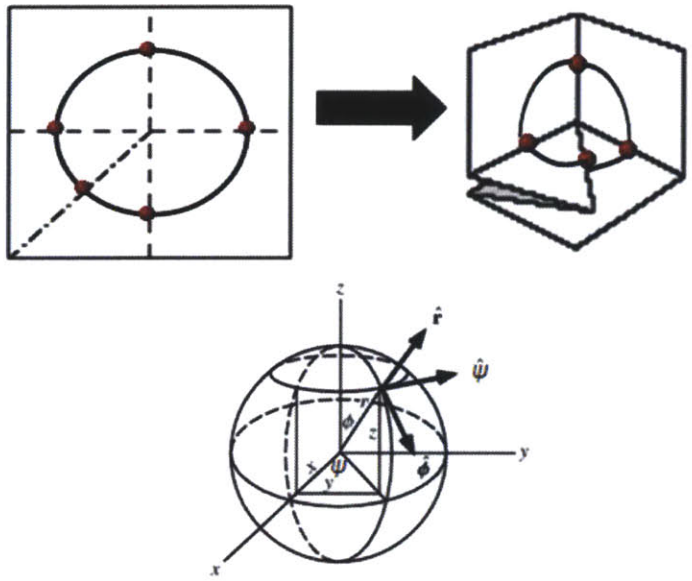

Figure 3-2: Crease pattern and folded corner cube.

nodes lie on the crease lines at unit length from the center vertex of the origami. Since the arc lengths are always kept at unit length from the center, every motion of an arc is exactly along the unit sphere. Fig. 3-2 illustrates the model in both the flat and folded states for the corner cube, and it shows the spherical coordinate frame used in the calculations.

Both the nodes of the bars (shown in red in Fig. 3-2) and the midpoints of each spherical arc are represented mathematically as unit, positive, electrostatic charges. The electrostatic potential induces a global energy field that tends to repel nodes from the arcs until the energy is minimized by following the steepest descent of energy. This expansive unfolding is analogous to pumping a balloon full of air until the elastic energy balances the energy input during pumping.

[15] proposed a set of four criteria that an admissible energy function should meet to smoothly unfold a chain. The properties include charge, repulsive, separable, and continuous first and second derivatives. The charge property indicates that the energy function tends to infinity if any two bars cross. Repulsive means that the vertices should repel each other as the energy is minimized, and separable specifies that the components of the energy function should be independent.

The simulations reported in this chapter tested both admissible energy functions described above and energy functions that met only the repulsive and continuity requirements. The energy U is defined as

$$U = \sum_{\substack{arc\ e \\ edge\ v \notin e}} \frac{1}{\gamma(v,e)^p} \tag{3.1}$$

for the separable case and

$$U = \frac{1}{\sum_{\substack{arc\ e \\ edge\ v \notin e}} \gamma(v,e)^p} \tag{3.2}$$

for the case of the non-separable energy. γ represents the geodesic distance along the unit sphere between each node and the center of every non-adjacent spherical arc, where p is a positive, real number. In our solution, $p = 2$ and $p = 4$ produced the smoothest results for the separable and non-separable functions, respectively. Although the energy could be calculated in terms of the Euclidean distance, we used the geodesic distance to take advantage of the spherical parameterization. It is also interesting to note that both separable and non-separable energy functions led the origami to unfold, but each encountered a few local minima, especially in the case of the corner cube. In practice, these local minima should not affect the physical folding operation, because the origami could be reduced to a one degree-of-freedom system by selectively actuating the flaps. Since this 1-DOF structure can be folded using only one actuator, there is no kinematic redundancy to complicate the folding motions.

The geodesic distance along the sphere was calculated using the cosine rule of spherical trigonometry. Spherical coordinates are depicted in Fig. 3-2 above, and

$$\gamma(v,e) = \arccos\left[\cos(\phi_i)\cos(\phi_{i+1}) + \sin(\phi_i)\sin(\phi_{i+1})\cos(\psi_{i+1} - \psi_i)\right] \tag{3.3}$$

for an arc beginning at node v_i and terminating at node v_{i+1}. Thus, the folded state represents the maximum energy state because the distances between vertices and non-adjacent arcs is minimum. Numerical minimization of this energy results in the gradual unfolding of the origami.

The i^{th} arc length, which represents the size of the i^{th} origami segment, is also calculated using (3.3). $\mathbf{G} \in \mathbf{R}^{m\times 1}$ represents the arc length constraints for m origami segments, and λ_i are the Lagrange multipliers. The resulting constrained optimization problem is solved numerically

in MATLAB using the Kuhn-Tucker equations, which are

$$\begin{aligned} \nabla U(\phi,\psi) + \sum_{i=1}^{m} \lambda_i \cdot \nabla G_i(\phi,\psi) &= 0 \\ \lambda_i \cdot G_i(\phi,\psi) &= 0, \; i = 1,,m \\ \lambda_i &\geq 0. \end{aligned} \tag{3.4}$$

The properties of the unfolding algorithm are as follows [15]:

- It enforces the rigidity of origami flaps via constraint definitions.
- Minimum energy state is in the plane (a great circle).
- If final state is not in the plane, then initial folded state is either locked or not flat unfoldable.
- Origami unfolds continuously (with interpolations) and can be refolded by following the coordinates in reverse.
- Repulsive property ensures that origami does not self-intersect.

3.2 Simulation Results

The algorithm reported in this thesis tested both admissible energy functions and those that met only the repulsive and continuity requirements. The unfolding of three single-vertex origamis is shown below in the OpenGL renderings. Fig. 3-3 shows the unfolding path of a piece of paper folded in half once. Fig. 3-4 depicts the unfolding of the corner cube origami, while Fig. 3-5 illustrates the trajectory of the water-bomb base.

One main result of interest is that origamis whose crease pattern is symmetric folded quite smoothly, but the asymmetric corner cube experienced local minima during the numerical minimization. Also, the fourth order energy function generates the smoothest unfolding trajectory. The fourth order term induces a steeper energy gradient and creates a smooth, non-oscillating trajectory.

Figure 3-3: Half-paper unfolding

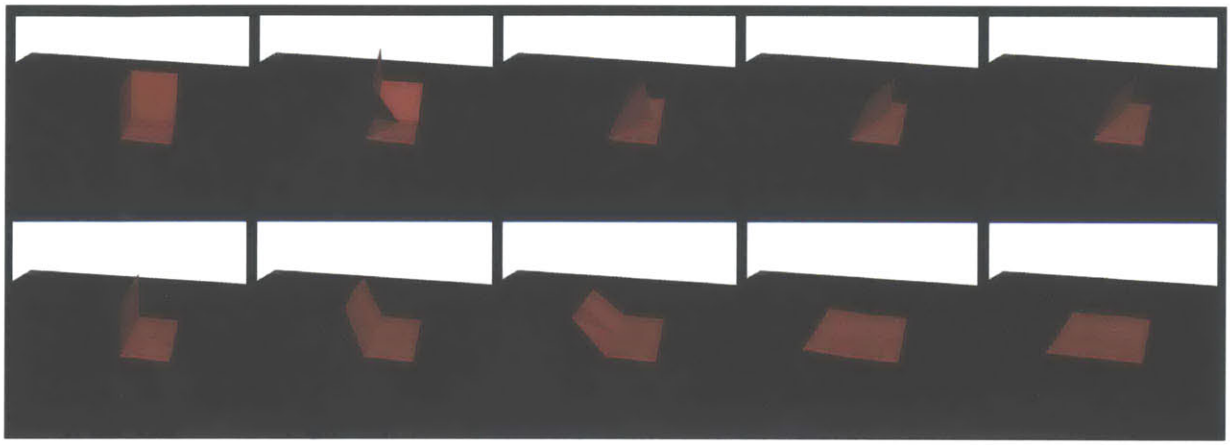

Figure 3-4: Unfolding of corner cube origami

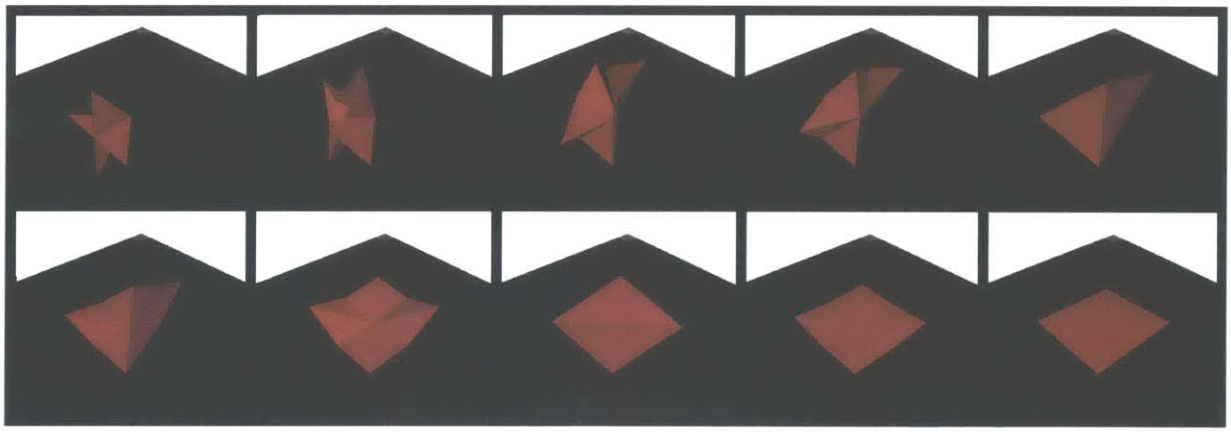

Figure 3-5: Water-bomb base unfolding path

We have shown that energy methods can be used to unfold single-vertex origamis, but the unfoldability of multiple-vertex origamis remains an open question. Perhaps similar methods can be used to understand the kinematics of these complex structures. The discussion in Chapter 6 will investigate possible avenues from which to approach this problem.

Chapter 4

Folding Dynamics

Modeling the dynamics of the actuation of Nanostructured Origami is essential to the successful and repeatable manufacturing of nanopatterned origamis, just as analytical modeling has streamlined the design of complex engineering systems such as integrated circuits and aircraft. The scalability of Nanostructured Origami is limited by our understanding of arbitrary geometries and of the dynamics of the actuation mechanisms. This thesis presents introductory research into the kinematic and dynamic modeling of accordion and single-vertex origami structures.

The dynamics of actuating nanopatterned origamis can be simulated based on methods developed within the robotics community. Each origami segment is modeled as a rigid body, and the creases are represented mathematically by revolute joints. Origami segments should remain rigid in order to maintain device integrity, which means that a stiff, strong material should be selected for the structural membrane. Since the creases allow only one rotational degree of freedom (DOF), the revolute joint model completely describes the relative motion of the segments. Screw calculus is then used to parameterize the motion of each segment's center of mass with respect to an inertial frame of reference. The equations of motion are formed using the relevant material properties, kinematics, and constraints, from which the trajectory is computed.

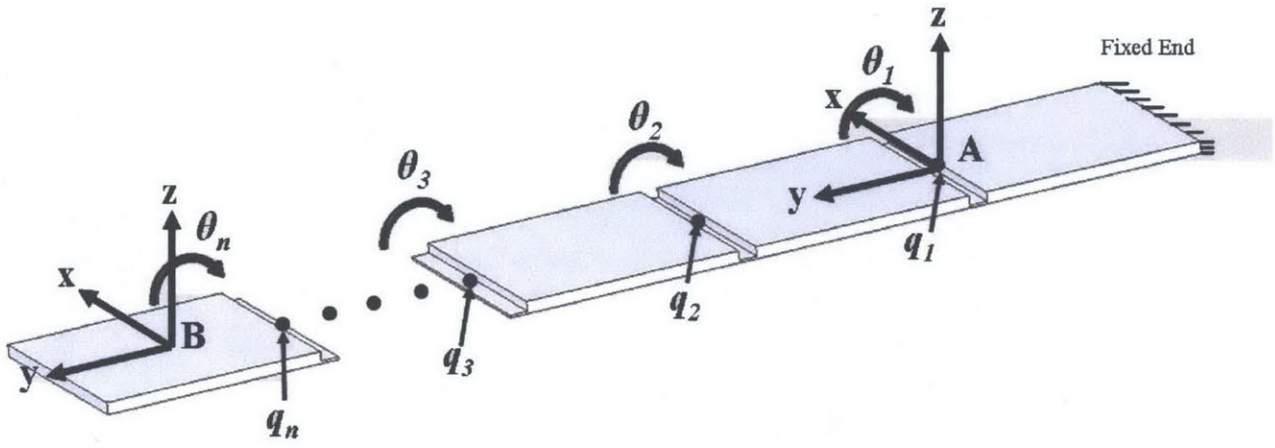

Figure 4-1: Schematic of n-link accordion origami.

4.1 Origami Topology

Origamis are folded about pre-defined axes called creases that are created within the material prior to folding. When folding paper, the creases are made simply by deforming the paper in the desired locations. For Nanostructured Origami, the creases are defined with a specific actuation method in mind. An accordion origami consists of a series of segments with the first link connected to ground and the last link free. If there are n 1-DOF creases, then the origami has n degrees of freedom. Fig. 4-1 shows the model for an accordion origami.

Many origamis, however, contain one or more closed kinematic chains. If the first and last links of an origami have a common ground, then that origami has a closed kinematic chain, or closed loop, topology. For these origamis, the number of degrees of freedom is not obvious since many creases may intersect. The closed loop nature of origami introduces dependencies between creases. Rotating one crease may produce rotations in several other creases, effectively creating a kinematic constraint condition on its configuration. An example of a closed chain, single vertex origami is shown in Fig. 4-2. The closed chain begins at A and loops around through Crease $n+1$ until the loop is closed again at A.

Another measure that is used to classify origamis is the number of interior vertices contained within the initially flat origami. A vertex is the point at which creases intersect. A

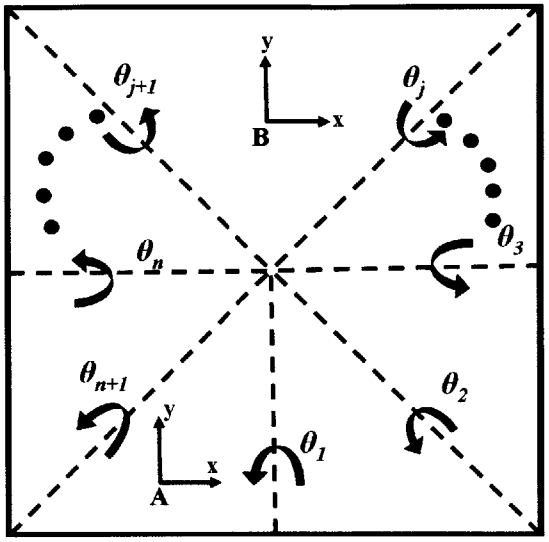

Figure 4-2: Schematic of arbitrary single-vertex origami

device with multiple vertices is more complex than one with a single interior vertex since there are dependencies not only between creases in the local kinematic chain but also between neighboring kinematic chains [21]. The most general Nanostructured Origami displays a closed loop topology, has multiple interior vertices, and contains segments of various shapes. This thesis calculates the dynamics of a set of rigid, closed chain origamis with only one interior vertex and one closed chain, such as the corner cube. Formulating the dynamic equations of motion for single vertex origamis is similar to the methods used for the accordions, but constraints must be introduced to account for the closed kinematic chain. These results can then be used as a basis for modeling more complicated structures with multiple vertices and several closed kinematic loops.

4.2 Kinematics

Consider an accordion origami with n creases and n links as shown in Fig. 4-1, and attach an inertial frame of reference A at the base of the origami and a body frame B at the center of mass of the n^{th} link. An accordion origami with n creases can be parameterized in terms of the crease angle θ_i between the i^{th} segment and the plane of the $(i-1)^{th}$ segment as shown

in Fig. 4-1. Screw calculus is then used to describe the configuration of a rigid body in space by defining an axis of rotation and a point $\mathbf{q} \in \mathbf{R}^3$ on that axis. Using the conventions and notation of screw theory defined in detail in [23], the configuration $\mathbf{g}_{AB} \in \mathbf{SE}(3)$ of frame B with respect to the inertial reference frame A is given by the product of exponentials formula

$$\mathbf{g}_{AB}(\theta) = e^{\hat{\boldsymbol{\xi}}_1\theta_1} e^{\hat{\boldsymbol{\xi}}_2\theta_2} \cdots e^{\hat{\boldsymbol{\xi}}_n\theta_n} \mathbf{g}_{AB}(0), \tag{4.1}$$

where $\mathbf{SE}(3)$ denotes the special Euclidean group. $\boldsymbol{\xi}_i \in \mathbf{R}^{4x4}$ represents the instantaneous twist axis for the i^{th} crease and is defined as

$$\boldsymbol{\xi}_i = \begin{bmatrix} \hat{\boldsymbol{\omega}}_i & -\boldsymbol{\omega}_i \times \mathbf{q}_i \\ 0 & 0 \end{bmatrix}. \tag{4.2}$$

The axis of rotation $\boldsymbol{\omega}_i$ is a three-dimensional vector, and the hat operator transforms the vector $\boldsymbol{\omega}_i$ into the skew-symmetric matrix

$$\hat{\boldsymbol{\omega}}_i = \begin{bmatrix} 0 & -\omega_z & \omega_y \\ \omega_z & 0 & -\omega_x \\ -\omega_y & \omega_x & 0 \end{bmatrix}, \tag{4.3}$$

which represents the vector cross product [23].

Screw theory is also used to calculate the velocity of a rigid body in space. The velocity of frame B with respect to frame A as viewed by an observer in the body frame is

$$\mathbf{V}_{AB} = \mathbf{J}_{AB}\dot{\boldsymbol{\theta}}. \tag{4.4}$$

The body Jacobian $\mathbf{J}_{AB} \in \mathbf{R}^{6\times n}$ which relates the crease velocities to the instantaneous body velocity is defined as

$$\mathbf{J}_{AB}(\theta) = \begin{bmatrix} \boldsymbol{\xi}_1^* & \boldsymbol{\xi}_2^* & \cdots & \boldsymbol{\xi}_n^* \end{bmatrix}, \tag{4.5}$$

and the body twists are

$$\boldsymbol{\xi}_i^* = Ad_{\left(e^{\hat{\xi}_1\theta_1} e^{\hat{\xi}_2} \cdots e^{\hat{\xi}_n} g_{AB}(0)\right)} \boldsymbol{\xi}_i. \tag{4.6}$$

The adjoint transformation Ad is an operator used to transform twists between coordinate

frames [23].

For a closed kinematic chain, the loop is cut such that there are two open chains that meet at a common coordinate frame B. Let frame B denote an "end-effector" located at the j^{th} segment of the origami as shown in the single vertex origami in Fig. 4-2. Chain 1 begins at the base frame A and consists of creases $i = 1 \cdots j$. Chain 2 also begins at A but contains Creases $i = n+1, n, \cdots j+1$. The loop equation for rigid origamis is given by the product of exponentials formula as

$$e^{\hat{\boldsymbol{\xi}}_1 \theta_1} \cdots e^{\hat{\boldsymbol{\xi}}_j \theta_j} \mathbf{g}_{AB}(0) = e^{\hat{\boldsymbol{\xi}}_{n+1} \theta_{n+1}} \cdots e^{\hat{\boldsymbol{\xi}}_{j+1} \theta_{j+1}} \mathbf{g}_{AB}(0). \tag{4.7}$$

This also introduces a constraint on the crease velocities for the two chains of the form

$$\begin{bmatrix} I \\ I \end{bmatrix} \mathbf{V}_{AB} = \begin{bmatrix} \mathbf{J}_1 & \mathbf{0} \\ \mathbf{0} & \mathbf{J}_2 \end{bmatrix} \dot{\boldsymbol{\theta}}, \tag{4.8}$$

where I is the identity matrix and $\mathbf{J}_i$ is the Jacobian for the i^{th} chain [23].

4.3 Constraints

The rigidity condition imposes constraints on the crease angles of closed chain origamis that must be included in the dynamic formulation. In general, an origami has $N = n - m$ degrees of freedom, where n is the number of creases and m is the number of holonomic constraints. Since the number of creases is typically greater than the number of degrees of freedom, only N creases need to be actuated by an external force, and m creases are simply passive creases in the origami. Consider a single vertex origami with $(n+1)$ creases and segments as shown in the 2-D crease pattern of Fig. 4-2. After virtually cutting one of the unactuated creases, the reduced system, or the virtual open chain, now has the form of an accordion origami with n generalized coordinates θ_i, $i = 1 \ldots n$. Let $\boldsymbol{\theta}^r \in \mathbf{R}^n$ represent the crease vector for the reduced open loop system. The n-dimensional vector of reduced system coordinates $\boldsymbol{\theta}^r$ is related to the closed chain system coordinates $\boldsymbol{\theta}^c \in \mathbf{R}^N$ by the holonomic constraint equation [23]

$$\boldsymbol{\theta}^r = \mathbf{f}(\boldsymbol{\theta}^c). \tag{4.9}$$

There are many methods for calculating the constraint relation $\mathbf{f}$. We determine $\mathbf{f}$ from (4.7) for origami structures analytically or numerically. The specific geometry dictates which method is used. A closed loop structure with a relatively simple geometry would be more amenable to an analytical approach than a complex device with multiple vertices and many closed chains. An example of an analytical method is illustrated in Chapter 5 for the corner cube. Finding the constraint relation automatically, however, is more readily accomplished using a numerical approach, as outlined in [29].

4.4 Open Chain Equations of Motion

The dynamic equations of motion for an accordion origami are derived using a Lagrangian technique, which is used to model the dynamics of open chain robotic manipulators. The Lagrangian L of a dynamic system is

$$L = T\left(\boldsymbol{\theta}, \dot{\boldsymbol{\theta}}\right) - V\left(\boldsymbol{\theta}\right), \tag{4.10}$$

where T is the system kinetic energy and V is the total potential energy of the system in terms of its generalized coordinates [30]. In terms of the kinetic and potential energy, the Newton-Euler equations of motion reduce to

$$\frac{d}{dt}\left(\frac{\partial L}{\partial \dot{\theta}_i}\right) - \frac{\partial L}{\partial \theta_i} = \tau_i, \tag{4.11}$$

where τ_i is the external torque applied to the i^{th} crease. Since the kinetic energy terms are the same for any open chain system with an arbitrary actuation method, it makes sense to break $\frac{\partial L}{\partial \theta_i}$ into the expression $\frac{\partial T}{\partial \theta_i} - \frac{\partial V}{\partial \theta_i}$. After simplifying (4.11), the equations of motion can be written in the usual matrix form as

$$\mathbf{M}\left(\boldsymbol{\theta}^r\right)\ddot{\boldsymbol{\theta}}^r + \mathbf{C}\left(\boldsymbol{\theta}^r, \dot{\boldsymbol{\theta}}^r\right)\dot{\boldsymbol{\theta}}^r + \mathbf{N}\left(\boldsymbol{\theta}^r, \dot{\boldsymbol{\theta}}^r\right) = \boldsymbol{\tau}^r. \tag{4.12}$$

From [23], the inertia matrix $\mathbf{M} \in \mathbf{R}^{n\times n}$ and Coriolis matrix $\mathbf{C} \in \mathbf{R}^{n\times n}$ arise from $\frac{d}{dt}\left(\frac{\partial T}{\partial \dot{\theta}_i}\right) - \frac{\partial T}{\partial \theta_i}$ since V is independent of $\dot{\theta}_i$. $\mathbf{M}$ and $\mathbf{C}$ are defined as

$$\mathbf{M}(\boldsymbol{\theta}) = \sum_{i=1}^{n} \mathbf{J}_i^T(\boldsymbol{\theta})\, \boldsymbol{\Phi}\, \mathbf{J}_i(\boldsymbol{\theta}) \tag{4.13}$$

and

$$\mathbf{C}\left(\boldsymbol{\theta}, \dot{\boldsymbol{\theta}}\right) = \frac{1}{2}\sum_{k=1}^{n}\left(\frac{\partial \mathbf{M}_{ij}}{\partial \theta_k} + \frac{\partial \mathbf{M}_{ik}}{\partial \theta_j} - \frac{\partial \mathbf{M}_{kj}}{\partial \theta_i}\right)\dot{\theta}_k,$$

where $\boldsymbol{\Phi}$ is the 6×6 inertia tensor given in [23]. $\boldsymbol{\tau}^r$ is the external torque vector applied to the generalized coordinates $\boldsymbol{\theta}^r$.

The $\mathbf{N}\left(\boldsymbol{\theta}, \dot{\boldsymbol{\theta}}\right)$ term on the left hand side of (4.12) includes generalized forces arising from the potential energy of the system as well as any non-conservative forces applied at the creases. In general, the potential energy of an origami is dependent on the strain energy in the hinges due to bending and can also be considered independent of the actuation method used. Of course, gravity should be included in the potential energy term, but simple calculations demonstrate that the strain energy due to bending a segment through an angle θ is orders of magnitude higher than the work done by gravity on such small masses. As an approximation, the bending is assumed to behave according to linear elastic deformation theory, which matches experimental results of at least one actuation method [11]. The elastic strain energy of a hinge is defined as potential energy of the form

$$V = \frac{1}{2E}\iiint_{\mu}[\sigma_{xx}^2 + \sigma_{yy}^2 + \sigma_{zz}^2 - 2\nu\left(\sigma_{xx}\sigma_{yy} + \sigma_{zz}\sigma_{yy} + \sigma_{xx}\sigma_{zz}\right) + 2\left(1+\nu\right)\left(\sigma_{yz}^2 + \sigma_{xz}^2 + \sigma_{yx}^2\right)]d\mu \tag{4.14}$$

where σ_{ij} is the ij component of the stress tensor, ν is the Poisson ratio, E is Young's modulus, and μ is the volume of the hinge [31]. In many instances, the expression for strain energy reduces significantly based on certain assumptions about the folding, and the bending mostly occurs about one axis. In [11], for example, the plane stress assumption reduced the bending equation to a one-dimensional problem as expected. For n hinges, the external moment vector $\mathbf{N}\left(\boldsymbol{\theta}, \dot{\boldsymbol{\theta}}\right) \in \mathbf{R}^n$ is related to the folding angle by the bending stiffness matrix $\mathbf{K} \in \mathbf{R}^{n\times n}$ by the

relationship

$$\mathbf{N}\left(\boldsymbol{\theta}^r, \dot{\boldsymbol{\theta}}^r\right) = \frac{\partial V}{\partial \boldsymbol{\theta}^r} + \boldsymbol{\tau}_{nc} = \mathbf{K}\boldsymbol{\theta}^r + \boldsymbol{\tau}_{nc}, \tag{4.15}$$

where $\boldsymbol{\tau}_{nc}$ is a vector of non-conservative forces applied to the creases. The strain in one crease is independent of the strain in another since the crease motions are independent, meaning that $\mathbf{K}$ is diagonal.

4.5 Closed Chain Equations of Motion

Following the research presented in [23],[27], and others as described in Chapter 2, we convert the closed chain origami into the original system and a reduced virtual open chain system. We define the closed chain torque vector $\boldsymbol{\tau}^c \in \mathbf{R}^N$ and the reduced open chain torque vector $\boldsymbol{\tau}^r \in \mathbf{R}^n$. The reduced system is assumed to undergo the same motions as the closed chain system, meaning that

$$\begin{aligned} \delta W^c &= \delta W^r, \\ &\text{or} \\ \boldsymbol{\tau}^c \cdot \delta\boldsymbol{\theta}^c &= \boldsymbol{\tau}^r \cdot \delta\boldsymbol{\theta}^r. \end{aligned} \tag{4.16}$$

Thus, the virtual work is equivalent for both systems since they undergo the same motions under the assumption of workless constraints. The differential form of (4.9) is

$$\begin{aligned} \dot{\boldsymbol{\theta}}^r &= \mathbf{G}\dot{\boldsymbol{\theta}}^c \\ &\text{or} \\ \delta\boldsymbol{\theta}^r &= \mathbf{G}\delta\boldsymbol{\theta}^c. \end{aligned} \tag{4.17}$$

The velocity constraint matrix $\mathbf{G} \in \mathbf{R}^{m\times N}$ that relates the open and closed chain virtual displacements is defined as

$$\mathbf{G} = \frac{\partial \mathbf{f}}{\partial \boldsymbol{\theta}}, \tag{4.18}$$

Expression (4.12) represents the system's equations of motion for the reduced open chain

origami, and the torques are related by substituting (4.17) into (4.16) [28]

$$\boldsymbol{\tau}^c = \mathbf{G}^T \boldsymbol{\tau}^r. \tag{4.19}$$

The reduced system equations of motion must be modified to account for the constraints so that the resulting dynamics represent the actual motion of the origami. Using the relationships in (4.19) and $\dot{\boldsymbol{\theta}}^r = \mathbf{G}\dot{\boldsymbol{\theta}}^c$, the closed chain equations of motion from [28] become

$$\boldsymbol{\tau}^c = \mathbf{G}^T[\mathbf{M}\left(\mathbf{f}\left(\boldsymbol{\theta}^c\right)\right)\left(\mathbf{G}\ddot{\boldsymbol{\theta}}^c + \dot{\mathbf{G}}\dot{\boldsymbol{\theta}}^c\right) + \mathbf{C}\left(\mathbf{f}\left(\boldsymbol{\theta}^c\right), \mathbf{G}\dot{\boldsymbol{\theta}}^c\right)\mathbf{G}\dot{\boldsymbol{\theta}}^c + \mathbf{N}\left(\mathbf{f}\left(\boldsymbol{\theta}^c\right), \mathbf{G}\dot{\boldsymbol{\theta}}^c\right)]. \tag{4.20}$$

Chapter 5

Examples

5.1 Accordion Origami

5.1.1 Geometry

The accordion origami is the simplest topological classification of origami. Potential applications of accordion-type Nanostructured Origamis include layered devices such as 3D photonic crystals [3] and bridge structures that are described in this example. A working electrochemical supercapacitor, which was built with an accordion topology, was successfully fabricated using Nanostructured Origami [7].

Although the equations defined in Chapter 4 are for any arbitrary actuation method, this example models the external forces and hinges used in the stress-based actuation method. In this procedure, a stressed material, such as chromium, is deposited on a relatively stress-free structural layer of silicon nitride. After the device is released from the substrate, the stressed material causes the structure to fold until the bending moment in the crease balances the moment caused by the initial stress. The radius of curvature ρ of the hinge is calculated as a function of material properties, geometry, and the initial stress in the material. Under the assumptions of linear deformation theory, the length l_i of the i^{th} hinge should be designed according to the simple kinematic relationship $l_i = \rho_i \theta_i$, where θ is again the turn angle of the segment [11]. Fig. 5-1 illustrates experimental results obtained from the stress actuation method. The three devices shown have an open kinematic chain topology with two hinges and

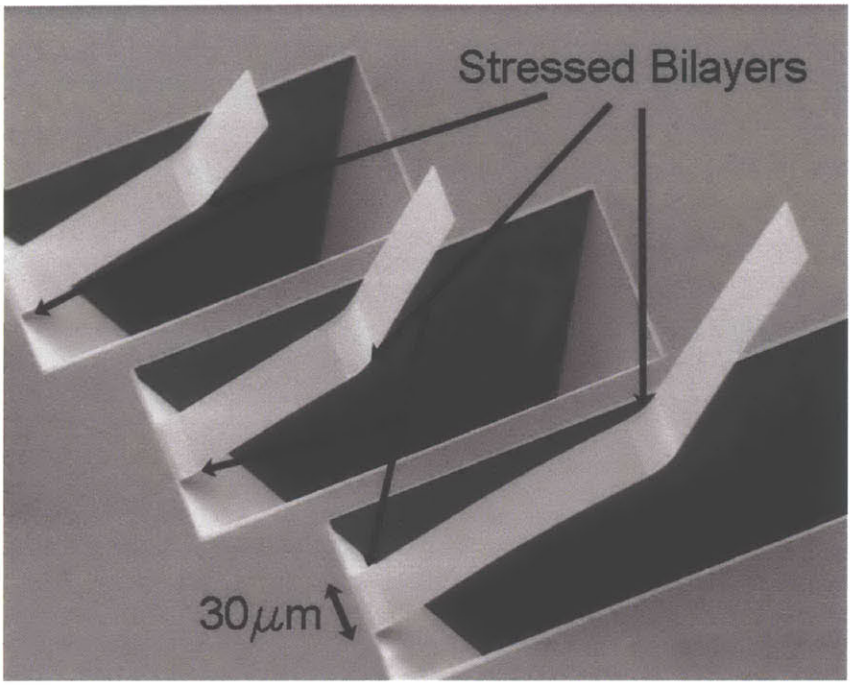

Figure 5-1: Accordion origamis actuated using a stressed bilayer.

two segments.

Consider the accordion origami crease pattern in Fig. 5-2a. This is a bridge-type structure which is commonly used in MEMS devices.

For example, in [32] the bridge was actuated vertically by electrostatic means to modulate the optical absorption in an underlying integrated optical circuit implementing a reconfigurable add-drop optical switch. Bridges such as this are usually manufactured by etching away a sacrificial layer; with the origami approach, a bridge could be manufactured according to the schematic in Fig. 5-2b. There are four creases and segments to be folded, and the creases and flaps are numbered consecutively from the base frame A. The axis of rotation $\boldsymbol{\omega}_i$ and the point

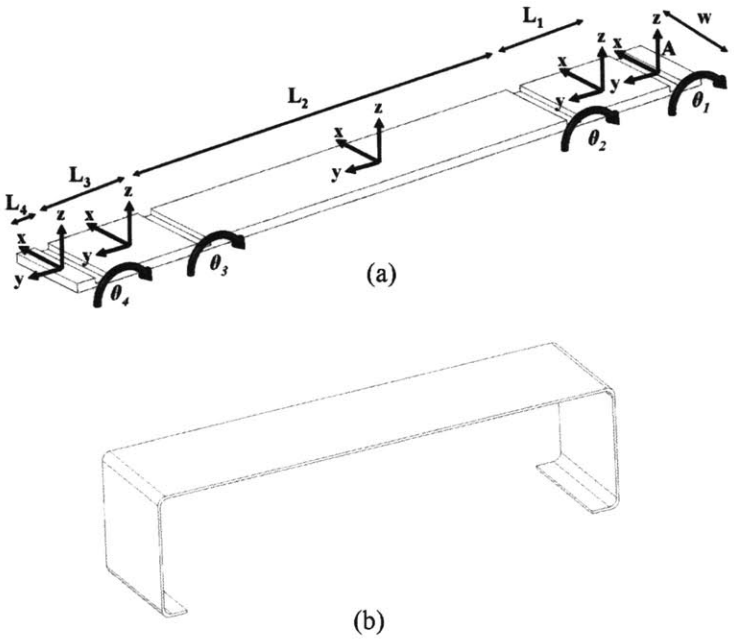

Figure 5-2: (a) Crease pattern of bridge device and (b) the bridge in its folded state.

on the axis $\mathbf{q}_i$ in microns are defined as

$$\boldsymbol{\omega}_1 = \boldsymbol{\omega}_2 = \boldsymbol{\omega}_3 = \boldsymbol{\omega}_4 = \begin{bmatrix} 1 \\ 0 \\ 0 \end{bmatrix} \tag{5.1}$$

$$\mathbf{q}_1 = \begin{bmatrix} 0 \\ 0 \\ 0 \end{bmatrix}, \mathbf{q}_2 = \begin{bmatrix} 0 \\ L_1 \\ 0 \end{bmatrix}, \mathbf{q}_3 = \begin{bmatrix} 0 \\ L_1 + L_2 \\ 0 \end{bmatrix}, \mathbf{q}_4 = \begin{bmatrix} 0 \\ L_1 + L_2 + L_3 \\ 0 \end{bmatrix}. \tag{5.2}$$

5.1.2 Equations of Motion

Following the general formulation outlined in Chapter 4, the open chain equations of motion can be defined according to (4.12), where $\mathbf{C}$ and $\mathbf{M}$ are both defined in (4.13). The generalized coordinates are shown in Fig. 5-1, and the vector representing these coordinates is

$$\boldsymbol{\theta}^r = \begin{bmatrix} \theta_1 \\ \theta_2 \\ \theta_3 \\ \theta_4 \end{bmatrix}. \tag{5.3}$$

The values of $\mathbf{J}_i(\boldsymbol{\theta})$, $\mathbf{M}(\boldsymbol{\theta})$, and $\mathbf{C}\left(\boldsymbol{\theta}, \dot{\boldsymbol{\theta}}\right)$ are defined in detail in Appendix A.

Consider the membrane bilayer shown in Fig. 5-3. Layer 1 is the structural layer, while layer 2 is pre-stressed.Of course, the Lagrangian could be computed such that the initial stress is included in the potential energy term, but, in order to maintain full generality, the stress will instead be included as an external torque term. The stiffness matrix $\mathbf{K}$ is then a diagonal matrix representing the bending stiffness of each hinge. In this example, all four creases are actuated, therefore each hinge is a bilayer. Based on the geometric assumptions in [11] with the additional condition of zero initial stress, the uni-axial stress distribution in layer j due to bending is

$$\sigma_{xx,j} = E'_j \frac{z}{\rho}. \tag{5.4}$$

$E'_j$is related to the elastic modulus E_j by $E'_j = \frac{E_j}{(1-\nu^2)}$. Now the potential energy in the hinge

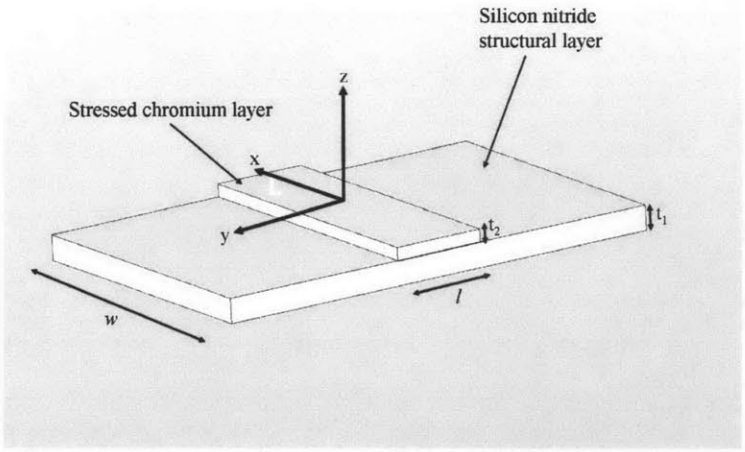

Figure 5-3: Diagram of thin film bilayer used in stress actuation technique.

can be calculated by substituting (5.4) into (4.14). The resulting expression

$$V_j = \frac{1}{2E} \iiint_{\mu} \left(E'_j \frac{z}{\rho} \right)^2 d\mu, \tag{5.5}$$

represents the energy stored in a hinge due to bending. Substituting the kinematic relationship $l_i = \rho_i \theta_i$ into (5.6), the resulting torque vector $\boldsymbol{\tau}_{bending} = \frac{\partial V}{\partial \boldsymbol{\theta}^r}$ is obtained as

$$\boldsymbol{\tau}_{bending} = \mathbf{K}\boldsymbol{\theta}^r, \tag{5.6}$$

where

$$\mathbf{K}_{11} = \mathbf{K}_{22} = \mathbf{K}_{33} = \mathbf{K}_{44} = \frac{w t_1^3 E_1}{3l\left(1-\nu_1^2\right)^2} + \frac{w t_2^3 E_2}{3l\left(1-\nu_2^2\right)^2} \tag{5.7}$$

for the bilayer hinges, and w denotes the width of the hinges.

A non-conservative drag force $\mathbf{B}\left(\boldsymbol{\theta}, \dot{\boldsymbol{\theta}}\right)$ is also included in the equations of motion to model damping due to the origami's motion through air. The drag force is given by $\mathbf{F}_i = \frac{1}{2} C_D \beta_{air} A \left|\mathbf{V}\right|^2 sgn(\mathbf{V} \cdot \hat{\mathbf{e}}_z) \hat{\mathbf{e}}_z$ where C_D, β_{air}, A, and $\hat{\mathbf{e}}_z$ represent the drag coefficient, air density, surface area and surface normal, respectively, and sgn is the signum function. Thus, $\mathbf{F}_i$ is the drag force applied at the i^{th} body's center of mass in the direction opposite that of the

body's velocity. This force is projected along the direction of the generalized force vector by

$$\tau_{nc} = \mathbf{J}_1^T \mathbf{F}_1 + \mathbf{J}_2^T \mathbf{F}_2 + \mathbf{J}_3^T \mathbf{F}_3 + \mathbf{J}_4^T \mathbf{F}_4, \tag{5.8}$$

where $\mathbf{J}_i$ is the body Jacobian of the i^{th} segment. The material properties and geometric parameters used in the stress actuation procedure are shown in Appendix A.

5.1.3 Forward Dynamics

Step Input

Upon deriving the equations of motion, the forward dynamics for an arbitrary input force can be simulated by numerically solving this second-order system of differential equations. For any actuation method applied to an origami, the step response describes the system's response to the immediate application of a set of generalized forces. Mathematically, this is represented by solving (4.12) for the input torque at steady state as

$$\tau^r = \mathbf{K}\boldsymbol{\theta}^r_\infty = \mathbf{K} \begin{bmatrix} \pi/2 \\ \pi/2 \\ \pi/2 \\ \pi/2 \end{bmatrix} \tag{5.9}$$

for the device shown in Fig. 5-2. Within the context of the stress actuation method, the step input represents the immediate release of the structural layer during the etch process.

We simulated the bridge origami using the material properties and geometry shown in Table 1 of Appendix A. The bilayer is composed of a structural silicon nitride membrane and the stressed chromium film. Since the sole source of damping in our model is drag, the system is underdamped. The segment trajectories overshoot and quickly collide. The trajectories of the segments as functions of time up to the first collision are shown in Fig. 5-4.

This result indicates that the instantaneous release is undesirable for this origami structure. Instead, in the next section, we consider a ramp model of gradual release which overcomes this problem.

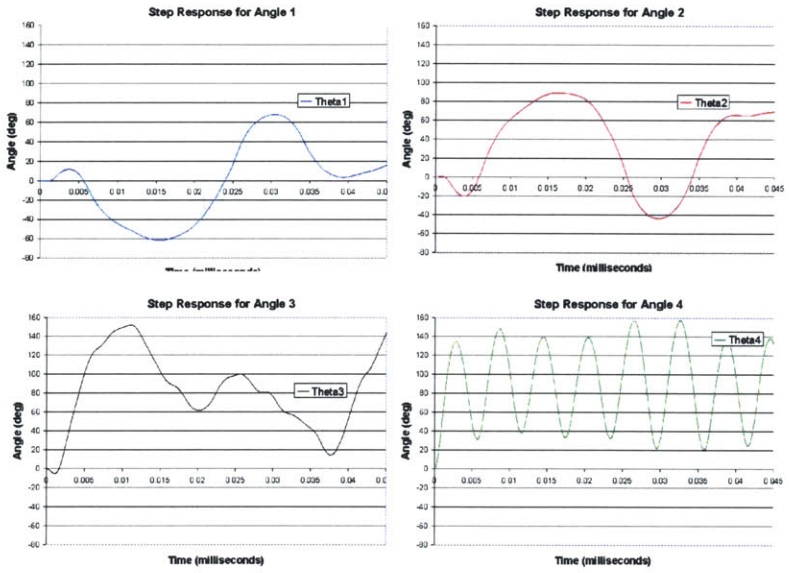

Figure 5-4: Step response of bridge device until collision.

Ramp Input

In practice, the release process is not immediate. Rather, the etch process occurs over a finite time period. For example, in [11], the devices were released using a potassium hydroxide (KOH) etch procedure. This highly directional etchant gradually releases the device from the silicon substrate as shown in the schematic of Fig. 5-5. Other methods of releasing the devices (such as UV or thermally-curable polyimides) might provide a faster actuation procedure, but the etch is still not immediate. The exact shape of the actuation waveform is not known for most cases. For the KOH etching, it can be modeled as a ramp, as we discuss in the remainder of this section. For other actuation methods, the ramp response calculation described here can still be useful, but it should be treated as an estimate only.

Consider the KOH etch process with etch rate α_i for the i^{th} hinge in the direction shown in Fig. 5-5. Since the etch in this case is along the length l_i of the i^{th} hinge, $\alpha_i = \frac{dl_i}{dt}$ represents the rate at which the hinge is released. By differentiating the kinematic constraint $l_i = \rho\theta_i$, we arrive at

$$\alpha_i = \frac{dl_i}{dt} = \rho\dot{\theta}_i. \tag{5.10}$$

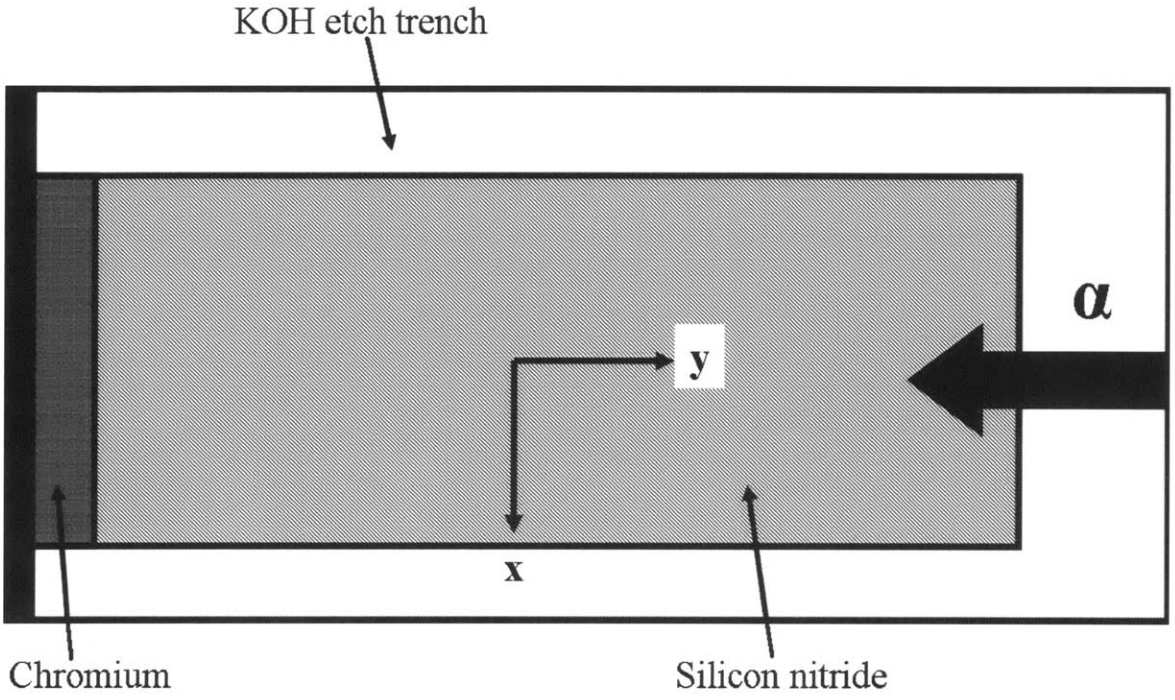

Figure 5-5: Schematic of KOH etch of single segment.

We can then integrate (5.10) to find θ_i by

$$\theta_{i,ramp} = \int_0^t \frac{\alpha}{\rho} dt = \begin{matrix} \frac{\alpha}{\rho} t \\ \frac{l_i}{\rho} \end{matrix} \left\{ \begin{array}{l} t \leq t_p \\ t > t_p \end{array} \right\}, \tag{5.11}$$

where $t_p = \rho\theta_{i,\infty}/\alpha$ is the time to completely underetch the hinge area of the origami. For the KOH etch procedure in [11], the release occurs over a timespan of several hours since $\alpha = 1.5\mu m/\min$. The mathematical model for a ramp input is

$$\boldsymbol{\tau}^r = \mathbf{C}\left(\boldsymbol{\theta}_{ramp}, \dot{\boldsymbol{\theta}}_{ramp}\right)\dot{\boldsymbol{\theta}}_{ramp} + \mathbf{B}\left(\boldsymbol{\theta}_{ramp}, \dot{\boldsymbol{\theta}}_{ramp}\right) + \mathbf{K}\boldsymbol{\theta}_{ramp}, \tag{5.12}$$

where $\boldsymbol{\theta}_{ramp}$ and $\dot{\boldsymbol{\theta}}_{ramp}$ represent the vector describing the kinematics of the ramp input for the KOH etch procedure. Solution of (5.12) over the time interval of 30 minutes leads to the response plots shown in Fig. 5-6. Fig. 5-7 illustrates the trajectory of the bridge device as it folds. Since there is no overshoot in Fig. 5-6, these results also indicate that there is no risk of collisions for this particular device when using the KOH etch. If other release methods are to be used in conjunction with the stress actuation method, then it is necessary to develop a suitable model of the release process and incorporate that into the input torque formulation.

5.1.4 Stability

After the folding operation has been completed, another important consideration is the stability of the device in its final configuration. For these devices, the equilibrium position is given by

$$\boldsymbol{\theta}_{eq} = \begin{bmatrix} \pi/2 \\ \pi/2 \\ \pi/2 \\ \pi/2 \end{bmatrix}. \tag{5.13}$$

In the simulations above, we used the value of ρ predicted in [11] based on the material properties of the chosen material system of SiN_x-Cr hinges. In equilibrium, $\theta_i = l_i/\rho$, so the desired equilibrium angles (5.13) can be guaranteed by properly selecting the hinge lengths. Moreover, since from (5.9) it can be seen that $\mathbf{K}$ is a positive definite matrix, the equilibrium

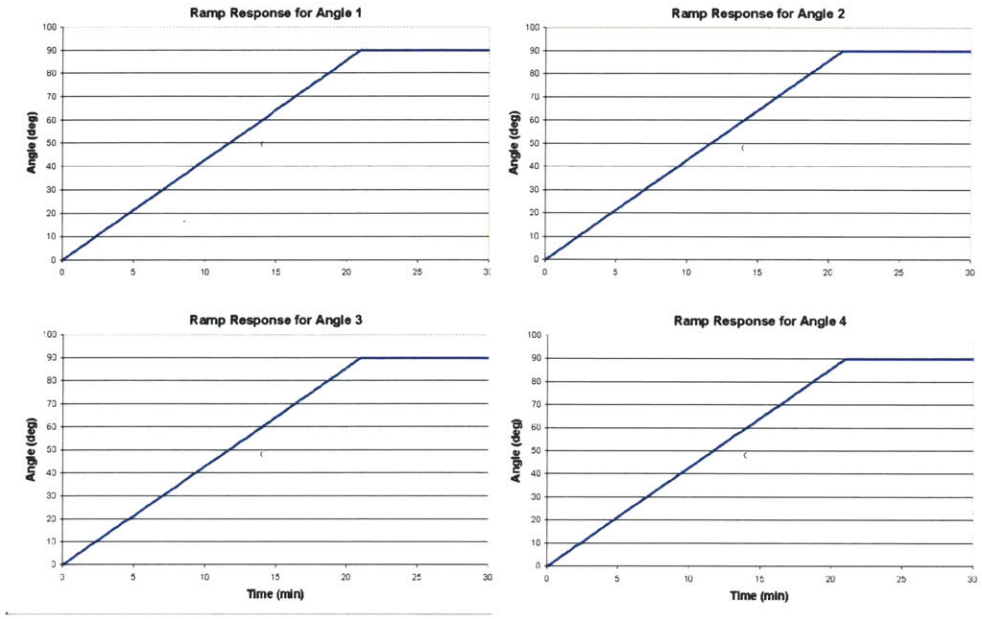

Figure 5-6: Ramp response plots for bridge device.

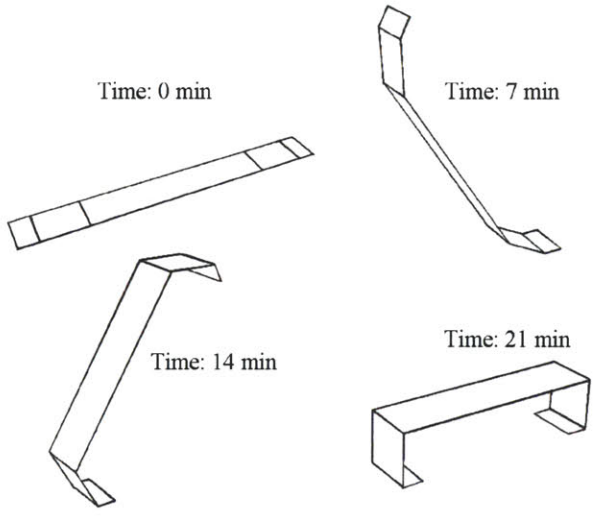

Figure 5-7: Trajectory of bridge resulting from ramp input.

is guaranteed to be stable.

We now proceed to evaluate the natural frequencies of the linearized system. Consider the steady state configuration of the bridge as shown in Fig. 5-2b. The linearized equations of motion are given by

$$\Delta\ddot{\boldsymbol{\theta}} + \mathbf{M}^{-1}\mathbf{K}\Delta\boldsymbol{\theta} = \mathbf{0}, \tag{5.14}$$

where $\Delta\boldsymbol{\theta}$ is the generalized displacement from equilibrium. The eigenvalues and eigenvectors of the folded system are of particular interest for control systems designed to maintain the final configuration. The eigenvalues of the positive definite matrix $\mathbf{A} = \mathbf{M}^{-1}\mathbf{K}$ are

$$\boldsymbol{\lambda} = 10^{12}\begin{bmatrix} 4.50 & 0 & 0 & 0 \\ 0 & 0.32 & 0 & 0 \\ 0 & 0 & 0.064 & 0 \\ 0 & 0 & 0 & 0.0024 \end{bmatrix}, \tag{5.15}$$

and the eigenvectors are the columns of the matrix

$$\mathbf{v} = \begin{bmatrix} 0.0127 & -0.1983 & 0.9495 & -1.0000 \\ -0.0204 & 0.2082 & -1.0000 & -0.9496 \\ 0.0870 & -1.0000 & -0.3962 & -0.00002 \\ -1.0000 & -0.0937 & -0.0020 & 0.0067 \end{bmatrix}. \tag{5.16}$$

The natural frequencies are found from (5.15) and are 337.6 kHz, 90 kHz, 40.4 kHz, and 7.88 kHz for the four modes of vibration. These frequencies are high in magnitude as expected since the masses of the membranes are very small compared to the crease stiffnesses. This is advantageous because the device will be robust to slow perturbations.

5.2 Corner Cube Origami

5.2.1 Geometry

The corner cube is a single vertex origami that is well-known within the origami mathematics community. It has been studied by [21] because it is one of few known origamis that can fold

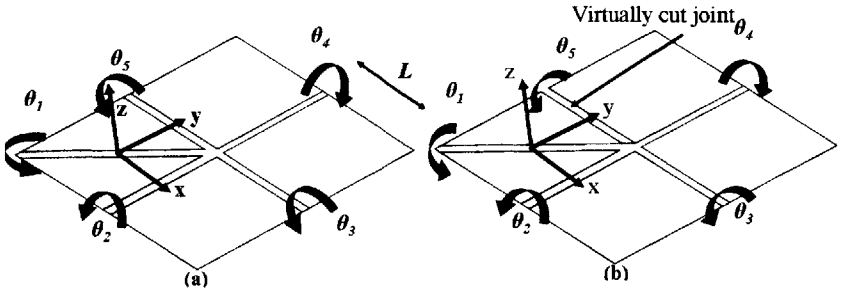

Figure 5-8: Schematic of (a) original closed chain corner cube and (b) reduced open chain system

rigidly. Besides being a mathematically interesting device, the corner cube is a useful optical device because it acts as a retroreflector to incident light.

The crease pattern of the corner cube is shown in Fig. 5-8a. In this figure, the closed chain is represented by the generalized coordinate vector $\boldsymbol{\theta} = \begin{bmatrix} \theta_1 & \theta_2 & \theta_3 & \theta_4 & \theta_5 \end{bmatrix}^T$. This parameterization of the corner cube, however, is not an independent set of generalized coordinates since the closed chain introduces kinematic constraints between the crease angles. Following the formulation defined in Chapter 4, the N degree of freedom closed chain system of Fig. 5-8a is converted into an equivalent virtual open chain by cutting the structure at Crease 5, which we select to be unactuated. Fig. 5-8b illustrates the virtual open chain system with n generalized coordinates defined by $\boldsymbol{\theta}^r = \begin{bmatrix} \theta_1 & \theta_2 & \theta_3 & \theta_4 \end{bmatrix}^T$.

The number of degrees of freedom N of a general spatial mechanism can be determined by the Grubler-Kutzbach criterion [33]

$$N = 6\,(r - p - 1) + \sum_{i=1}^{p} f_i, \tag{5.17}$$

where r is the number of rigid links, p is the number of creases, and f_i represents the number of degrees of freedom of the i^{th} crease. For the corner cube, (5.17) reduces to

$$N = 6\,(5 - 5 - 1) + \sum_{i=1}^{5} 1_i = -1. \tag{5.18}$$

The negative result in this case indicates that this origami is overdetermined [33],[22]. If one axis of rotation is locked, however, then the system is effectively converted into the familiar 1-DOF 4R overconstrained system that is well-understood in the robotics community [22]. Blocking the rotation axes in this manner naturally allows for a two-step actuation sequence:

Step 1 - Lock θ_2 and fold the 4R overconstrained subsystem 180° about θ_1

Step 2 - Lock θ_1 and fold the partially-folded origami 90° about θ_2.

Therefore, the corner cube can be modeled as a 2-DOF system described by θ_1 and θ_2 in which each degree of freedom is actuated in a separate step. For the stress actuation method, this implies that only Creases 1 and 2 require the stressed bilayer for actuation. The other three creases will be passive hinges that are kinematically dependent on the driving angles $\boldsymbol{\theta}^c$.

In the folding motion of Step 1, $N = 1$ since this is a 4R overconstrained system. Because θ_2 is locked during the first folding sequence, the reduced open chain coordinates are described by $\boldsymbol{\theta}^r = \begin{bmatrix} \theta_1 & \theta_3 & \theta_4 \end{bmatrix}$. Upon choosing $\boldsymbol{\theta}^c = [\theta_1]^T$ to be the independent generalized coordinate vector of the original closed chain system, it is evident that there are $m = 2$ holonomic constraints relating $\boldsymbol{\theta}^r$ to $\boldsymbol{\theta}^c$ by (4.9).

Previous work [22] determined the holonomic constraint relation for the corner cube. Those results are briefly illustrated in Chapter 2. The constraint $\mathbf{f}$ is calculated by a virtual cut at Crease 5 for the first fold. The two kinematic chains stemming from the base frame A and resulting from the cut have an open chain topology. Crease 1 from the first chain is the input angle which is perturbed by a known angle, and the configuration of the end effector at Crease 5 is computed using (4.1).

The inverse kinematics chain also begins at Crease 1 but traverses the opposite direction through Creases 2, 3, and 4. (4.7) is used to solve the inverse kinematics problem to find the change in the output angles θ_3 and θ_4 due to the perturbation at θ_1. The input-output relationship that is found from the loop closure equations allows for the determination of $\mathbf{f}$ in (5.19) which is described graphically in Fig. 5-9. Although an expression relating $\boldsymbol{\theta}^r$ and $\boldsymbol{\theta}^c$ is generally difficult to determine analytically, a fourth order polynomial curve fitting technique was employed to obtain an approximate analytical relationship between the coordinates in

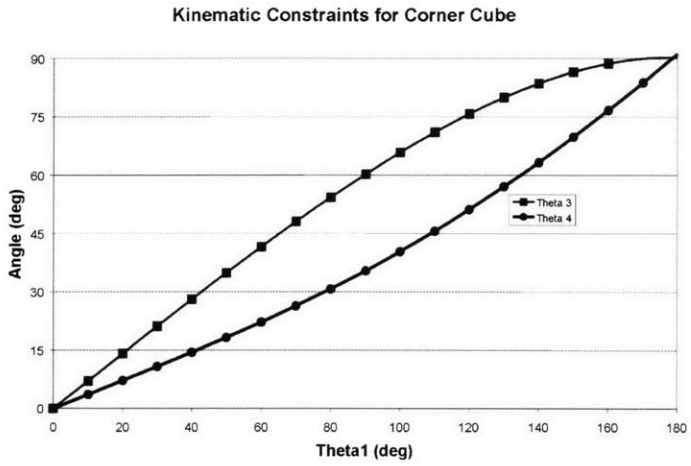

Figure 5-9: Holonomic constraint relation for corner cube

degrees given by [22]

$$\begin{aligned} \boldsymbol{\theta}^r &= \mathbf{f}(\boldsymbol{\theta}^c); \\ \begin{bmatrix} \theta_1 \\ \theta_3 \\ \theta_4 \end{bmatrix} &= \begin{bmatrix} \theta_1 \\ a_{31}\theta_1^4 + a_{32}\theta_1^3 + a_{33}\theta_1^2 + a_{34}\theta_1 + a_{35} \\ a_{41}\theta_1^4 + a_{42}\theta_1^3 + a_{43}\theta_1^2 + a_{44}\theta_1 + a_{45} \end{bmatrix} \end{aligned} \tag{5.19}$$

where the constant coefficients are found in Table 2.

	a_{3k} (deg)	a_{4k} (deg)
$k=1$	$-1.8\,(10^{-8})$	$-2.4\,(10^{-8})$
$k=2$	$-3\,(10^{-6})$	$1.2\,(10^{-5})$
$k=3$	$3.1\,(10^{-5})$	$-6.2\,(10^{-4})$
$k=4$	0.71	0.37
$k=5$	0.0089	-0.015

Table 2. Polynomial coefficients for constraint relations

To parameterize the corner cube using screw calculus, the twist axes and the points on those axes must be defined as described in Chapter 4. For the device in Fig. 5-8b, $\boldsymbol{\omega}_i$ and $\mathbf{q}_i$ (in

microns) are given by

$$\boldsymbol{\omega}_1 = \begin{bmatrix} -1 \\ -1 \\ 0 \end{bmatrix}, \boldsymbol{\omega}_3 = \begin{bmatrix} 1 \\ 0 \\ 0 \end{bmatrix}, \boldsymbol{\omega}_4 = \begin{bmatrix} 0 \\ 1 \\ 0 \end{bmatrix}, \tag{5.20}$$

and

$$\mathbf{q}_1 = \begin{bmatrix} 0 \\ 0 \\ 0 \end{bmatrix}, \mathbf{q}_3 = \begin{bmatrix} L \\ L/2 \\ 0 \end{bmatrix}, \mathbf{q}_4 = \begin{bmatrix} L/2 \\ L \\ 0 \end{bmatrix}.$$

5.2.2 Equations of Motion

Consider the virtual open chain origami of Fig. 5-8b. In this reduced system, each angle of $\boldsymbol{\theta}^r$ is modeled as having a virtual actuator attached to every crease. The equations of motion for this open kinematic chain are given by (4.12), where $\mathbf{M}$ and $\mathbf{C}$ are still defined by (4.13). The values for the reduced system matrices $\mathbf{J}_i$, $\mathbf{M}$, and $\mathbf{C}$ are given in Appendix B. Similarly, $\boldsymbol{\tau}_{nc} = \mathbf{J}_1^T\mathbf{F}_1 + \mathbf{J}_3^T\mathbf{F}_3 + \mathbf{J}_4^T\mathbf{F}_4$, and the stiffness matrix $\mathbf{K}$ is a 3×3 diagonal matrix with entries K_{ij} defined by

$$\begin{aligned} \mathbf{K}_{11} &= \frac{wt_1^3E_1}{3l_1\left(1-\nu_1^2\right)^2} + \frac{wt_2^3E_2}{3l_1\left(1-\nu_2^2\right)^2}, \\ \mathbf{K}_{22} &= \mathbf{K}_{33} = \frac{wt_1^3E_1}{3l_2\left(1-\nu_1^2\right)^2}. \end{aligned} \tag{5.21}$$

Because creases 3 and 4 are unactuated, the length l_2 of the unstressed hinges can be set arbitrarily to minimize the radius of curvature of the creases. The dynamics of the virtual open chain, in terms of $\boldsymbol{\theta}^r$, is described precisely by this system of three ordinary differential equations originally presented in (4.12).

5.2.3 Forward Dynamics

Step Input

In order to simulate the dynamics of the corner cube, it is first necessary to calculate the input generalized torque $\boldsymbol{\tau}^c \in \mathbf{R}^{1\times 1}$ applied to Crease 1 as outlined in [26],[27]. The reduced system virtual torque $\boldsymbol{\tau}^r \in \mathbf{R}^{3\times 1}$ is determined by

$$\boldsymbol{\tau}^r = \mathbf{K}\boldsymbol{\theta}^r_\infty = \mathbf{K}\begin{bmatrix} \pi \\ \pi/2 \\ \pi/2 \end{bmatrix} \tag{5.22}$$

for a step input with virtual actuators attached to Creases 3 and 4. (5.22) represents the virtual open chain dyamics, but the open chain parameterization does not account for the closed loop constraints. The closed chain input torque $\boldsymbol{\tau}^c$ is related to $\boldsymbol{\tau}^r$ by the constraint Jacobian $\mathbf{G} \in \mathbf{R}^{3\times 1}$ by

$$\begin{aligned} \boldsymbol{\tau}^c &= \mathbf{G}^T\boldsymbol{\tau}^r, \\ \boldsymbol{\tau}^c &= \begin{bmatrix} 1 & \frac{\partial\theta_3}{\partial\theta_1} & \frac{\partial\theta_4}{\partial\theta_1} \end{bmatrix}\boldsymbol{\tau}^r, \end{aligned} \tag{5.23}$$

where the partial derivatives in $\mathbf{G}^T$ can be found simply from the quartic holonomic constraints in $\mathbf{f}$.

Let l_i^c denote the longer hinge length associated with the closed chain such that the compliance of the crease results in the requisite amount of torque. One way to determine l_i^c is to use a concept of "torque magnification", which describes the magnification on the open chain torque that is required to actuate the closed chain. Let τ_1^o and τ_1^c be the torques required to actuate Crease 1 of the virtual open chain and the closed chain systems, respectively. Then, we define the torque magnification factor η as

$$\eta = \frac{\tau_1^c}{\tau_1^o}. \tag{5.24}$$

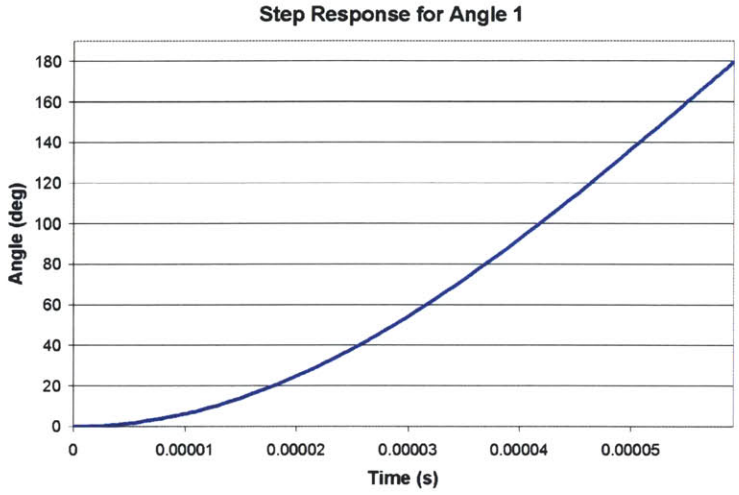

Figure 5-10: Step response of corner cube until collision.

This value can be used to approximate the new value of the stiffness k_1' for Crease 1 as

$$k_1' = \frac{k_1}{\eta}. \tag{5.25}$$

Finally, the longer hinge length l_i^c can be found from (5.7). This value is then substituted into the equations of motion (4.20).

The geometric parameters for the corner cube used in this simulation are shown in Table 3 of Appendix B. Fig. 5-10 plots the step response of Crease 1 until collision for the corner cube origami resulting from the input torque $\boldsymbol{\tau}^c$. Again, the response plots show that collisions occur, which indicates that a ramp input model is more accurate. The preceding discussion describes the dynamics of actuating Step 1 of the actuation sequence. Since θ_3, θ_4, and the cut angle θ_5 have reached the folded state, the resulting partially folded origami has 1-DOF about θ_2 which can be easily modeled without constraints according to the analysis above..

5.2.4 Ramp Input

Following the arguments above regarding etch rates, a more accurate input torque model

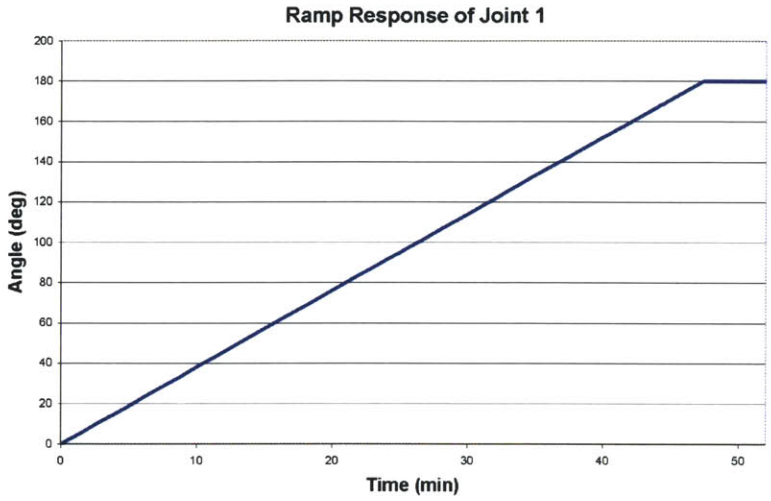

Figure 5-11: Ramp response of corner cube

for the stress actuation technique is defined by a ramp input to the active creases. For a closed kinematic chain, this is expressed as

$$\boldsymbol{\tau}^c = \mathbf{G}^T \boldsymbol{\tau}^r = \mathbf{G}^T \left(\mathbf{C} \left(\boldsymbol{\theta}_{ramp}, \dot{\boldsymbol{\theta}}_{ramp} \right) \dot{\boldsymbol{\theta}}_{ramp} + \mathbf{B} \left(\boldsymbol{\theta}_{ramp}, \dot{\boldsymbol{\theta}}_{ramp} \right) + \mathbf{K} \boldsymbol{\theta}_{ramp} \right). \tag{5.26}$$

The response plots are illustrated in Fig. 5-11, and a schematic of the folding of the corner cube can be seen in Fig. 5-12. The first three plots illustrate the motions for Step 1, while the last shows the final folding motion of Step 2. The response exhibits minimal overshoot compared to the step response. This indicates that the ramp input model for the stress actuation procedure predicts no risk of serious collisions between the segments.

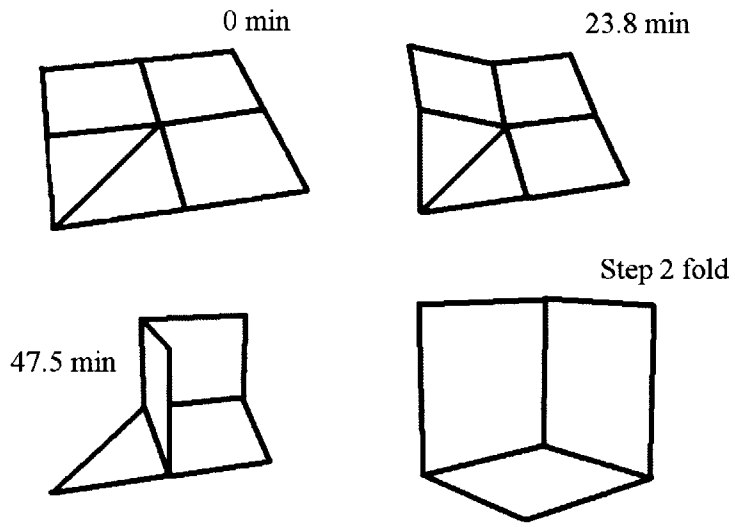

Figure 5-12: Trajectory of corner cube resulting from a ramp input.

5.2.5 Stability

The final folded configuration of the corner cube is shown in Fig. 5-12, where the equilibrium crease angles of the closed chain are defined as

$$\boldsymbol{\theta}_{eq} = \begin{bmatrix} \theta_1 \\ \theta_2 \\ \theta_3 \\ \theta_4 \end{bmatrix} = \begin{bmatrix} \pi \\ \pi/2 \\ \pi/2 \\ \pi/2 \end{bmatrix}. \tag{5.27}$$

The folded configuration has 2-DOF with θ_1 and θ_2 again as the generalized coordinates of the device. (4.20) is linearized about the equilibrium point subject to the constraints of (5.19) since small motions about equilibrium must still obey the constraints. The nonlinear drag force is again neglected at equilibrium in the equations of motion, and the Coriolis matrix disappears as described in detail in [30]. The resulting system of two differential equations is

$$\Delta\ddot{\boldsymbol{\theta}}^c + \mathbf{M}^{-1}\mathbf{K}\Delta\boldsymbol{\theta}^c = \mathbf{0}. \tag{5.28}$$

The eigenvalues are given by

$$\lambda = 10^9 \begin{bmatrix} 0.29 & 0 \\ 0 & 3.3 \end{bmatrix}, \tag{5.29}$$

while the associated eigenvectors are the columns of

$$\mathbf{v} = \begin{bmatrix} -0.986 & 0.35 \\ -0.166 & -0.94 \end{bmatrix}. \tag{5.30}$$

The natural frequencies are given by 2.7 kHz and 9.1 kHz.

Since the stiffness matrix is positive definite, the corner cube is indeed at a stable equilibrium. In fact, one of the principle benefits of the stress actuation method is that the final folded state will always be at a stable equilibrium since the stiffness matrix is always a square, positive, diagonal matrix. The inherent mechanics of the process ensure that the torque due to the stressed membrane is always stably balanced by the bending moment.

Chapter 6

Conclusions and Future Work

This thesis presents modeling techniques that can be used to simulate the actuation of Nanostructured Origami devices. The analytical methods are based on the large body of information available on origami mathematics and robotics. The primary achievements relate to the geometry and physics of the folding and unfolding of single-vertex and accordion origamis. It is expected that this research will lay the foundation for the simulation of more complex origamis.

6.1 Single-Vertex Unfolding

The rigid unfolding of single-vertex origamis has been demonstrated. The unfolding trajectories of the half-paper, corner cube, and waterbomb base were simulated using energy methods that were previously explored in [15]. A constrained optimization routine was implemented to calculate the trajectories numerically, and the kinematic constraints can then be extracted from the results. The direct extension of energy methods to the unfolding and kinematics of multiple vertex origamis is unknown, but it presents interesting research questions to pursue.

6.2 Simulation of Origami Dynamics

A generic formulation for modeling the dynamics of Nanostructured Origami has been presented based on techniques that are widely used to model robotic manipulators. We extend these methods to model origamis with open kinematic chains and those containing one closed

kinematic chain (i.e. a single interior vertex). The input generalized forces necessary to actuate the origamis were calculated, and the forward dynamics were simulated for both a generic actuation method and for the stress actuation procedure. The response of a ramp input for both types of origamis is very-well behaved, as there is no overshoot due to the slow etching rate. For stress actuation, it was also verified that since the stiffness matrix is always positive definite at an equilibrium position, the final folded configuration is stable. The same principles can be used to calculate the dynamics of origamis with multiple interior vertices and closed kinematic chains, but determining the kinematic constraint relations will inevitably be more complex.

6.3 Future Work

Nanostructured Origami offers great promise as an effective 3D nanomanufacturing process. Besides the theoretical investigations outlined in this thesis, several actuation mechanisms have been successfully tested, and a working origami device [7] has been fabricated. Other researchers in the 3D Optics group at MIT are actively investigating precision alignment techniques and latching mechanisms that can be used to accurately position the devices in the folded state. Thus, there are exciting directions in which we can further develop the technology.

From the theoretical front, the following modeling tools should be developed:

- Software suite - In order to expedite the design process for an arbitrary origami, the modeling techniques described here should be implemented in an extensive software tool. [22] developed a software tool using Visual Basic for simulating the corner cube. The dynamic modeling capabilities are now being integrated with the kinematics in a new software suite using Microsoft's C# language. When further theoretical developments are made, they will also be added to the software so that the origami design process is automated.

- Experimental verification - It is imperative that the dynamic models are tested in the lab on folding origamis. Various types of sensors can be used to track the trajectory as the origami folds, and the results will be compared to the analytical results.

- Control schemes - Theoretical and experimental control strategies should be explored in

order to make the actuation process more robust. Feedback will improve the plant model of the actuation scheme, and the placement of the origami segments will be more accurate.

- Multiple vertex origamis - Little is known about the geometry of multiple vertex origamis. The ultimate objective is to be able to transform a 3D design from the concept stage to a working crease pattern for the Nanostructured Origami technique. Optimization routines such as the energy method offer promising results for understanding these origamis. Perhaps a similar method will help in solving the unfolding of rigid multiple vertex origamis. Pseudo-triangulation is also a promising technique for investigating origamis with multiple vertices. The 1-DOF motion is an attractive strategy since the unfolding motion is simplified considerably.

Part I

Appendix A: Geometric and Material Parameters for Bridge

Parameter	Value	Units
ρ	20	μm
l	32	μm
w	100	μm
t_1	0.2	μm
t_2	0.1	μm
E_1	300	GPa
E_2	140	GPa
ν_1	0.28	–
ν_2	0.21	–
β_m	3.27E-12	$g/\mu m^3$
L_1	100	μm
L_2	400	μm
L_3	100	μm
L_4	20	μm

Table 1. Parameters for bridge devie

The Jacobians, mass and Coriolis matrices for the bridge origami are shown below. s_i and c_i represent sin and cos of the i^{th} joint, and β_m is the mass density of the silicon nitride structural material.

$$\mathbf{J}_1 = \begin{bmatrix} 0 & 0 & 0 & 0 \\ 0 & 0 & 0 & 0 \\ L_1/2 & 0 & 0 & 0 \\ 1 & 0 & 0 & 0 \\ 0 & 0 & 0 & 0 \\ 0 & 0 & 0 & 0 \end{bmatrix}$$

$$\mathbf{J}_2 = \begin{bmatrix} 0 & 0 & 0 & 0 \\ L_1 s_2 & 0 & 0 & 0 \\ L_1 c_2 + L_2/2 & L_2/2 & 0 & 0 \\ 1 & 1 & 0 & 0 \\ 0 & 0 & 0 & 0 \\ 0 & 0 & 0 & 0 \end{bmatrix}$$

$$\mathbf{J}_3 = \begin{bmatrix} 0 & 0 & 0 & 0 \\ L_1 s_3 c_2 + L_1 s_2 c_3 + L_2 s_3 & L_2 s_3 & 0 & 0 \\ L_1 c_3 c_2 + L_2 c_3 - L_1 s_2 s_3 + L_3/2 & L_2 c_3 + L_3/2 & L_3/2 & 0 \\ 1 & 1 & 1 & 0 \\ 0 & 0 & 0 & 0 \\ 0 & 0 & 0 & 0 \end{bmatrix}$$

$$\text{column 1 of } \mathbf{J}_4 : \begin{bmatrix} 0 \\ c_2 c_4 s_3 L_1 + c_2 s_4 c_3 L_1 + \\ s_2 c_4 c_3 L_1 + c_4 s_3 L_2 + \\ s_4 c_3 L_2 - s_2 s_4 s_3 L_1 + s_4 L_3 \\ \\ 1/2 L_4 + c_4 L_3 + c_2 c_4 c_3 L_1 - \\ c_2 s_4 s_3 L_1 - s_2 c_4 s_3 L_1 - \\ s_2 s_4 c_3 L_1 + c_4 c_3 L_2 - s_4 s_3 L_2 \\ 1 \\ 0 \\ 0 \end{bmatrix}$$

$$\text{column 2 of } \mathbf{J}_4 : \begin{bmatrix} 0 \\ c_4 s_3 L_2 + s_4 c_3 L_2 \\ +s_4 L_3 \\ c_4 c_3 L_2 + c_4 L_3 + \\ 1/2 L_4 - s_4 s_3 L_2 \\ 1 \\ 0 \\ 0 \end{bmatrix}$$

$$\text{columns 3 and 4 of } \mathbf{J}_4 : \begin{bmatrix} 0 & 0 \\ s_4 L_3 & 0 \\ c_4 L_3 + 1/2 L_4 & L_4/2 \\ 1 & 1 \\ 0 & 0 \\ 0 & 0 \end{bmatrix}$$

$$\begin{aligned} \mathbf{M}_{11} = \; & 1/4 L_1^3 \beta_m w t_1 + 1/12 \beta_m L_1 w^3 t_1 + 1/12 \beta_m L_1 w t_1^3 + \\ & 1/12 \beta_m L_2 w t_1 (12 L_1^2 + 12 L_1 c_2 L_2 + 3 L_2^2 + w^2 + t_1^2) + \\ & 1/12 \beta_m L_3 w t_1 (24 L_1 c_2 L_2 + 12 L_2^2 + 12 c_3 L_1 c_2 L_3 + \\ & 12 c_3 L_2 L_3 + 12 L_1^2 - 12 s_3 L_1 s_2 L_3 + 3 L_3^2 + w^2 + \\ & t_1^2) + 1/12 \beta_m L_4 w t_1 (t_1^2 + w^2 + 3 L_4^2 + 12 L_2^2 + \\ & 12 L_4 c_4 L_3 + 12 L_1^2 + 24 L_1 c_2 L_2 + 12 L_4 c_2 c_4 c_3 L_1 \\ & -12 L_4 c_2 s_4 s_3 L_1 - 12 L_4 s_2 c_4 s_3 L_1 - 12 L_4 s_2 s_4 c_3 L_1 \\ & +12 L_3^2 + 24 c_3 L_2 L_3 + 24 c_3 L_1 c_2 L_3 - 24 s_3 L_1 s_2 L_3 \\ & +12 L_4 c_4 c_3 L_2 - 12 L_4 s_4 s_3 L_2) \end{aligned}$$

$$
\begin{aligned}
\mathbf{M}_{12} &= 1/12\beta_m L_2 w t_1(6L_1c_2L_2 + 3L_2^2 + w^2 + t_1^2) + \\
&\quad 1/12\beta_m L_3 w t_1(12L_1c_2L_2 + 12L_2^2 + 6c_3L_1c_2L_3 + \\
&\quad 12c_3L_2L_3 - 6s_3L_1s_2L_3 + 3L_3^2 + w^2 + t_1^2) + \\
&\quad 1/12\beta_m L_4 w t_1(-12s_3L_1s_2L_3 + 12c_3L_1c_2L_3 + \\
&\quad 12L_1c_2L_2 + t_1^2 + w^2 + 3L_4^2 + 24c_3L_2L_3 + 12L_2^2 + \\
&\quad 12L_4c_4L_3 + 6L_4c_2c_4c_3L_1 - 6L_4c_2s_4s_3L_1 \\
&\quad -6L_4s_2c_4s_3L_1 - 6L_4s_2s_4c_3L_1 + 12L_3^2 + \\
&\quad 12L_4c_4c_3L_2 - 12L_4s_4s_3L_2)
\end{aligned}
$$

$$
\begin{aligned}
\mathbf{M}_{13} &= 1/12\beta_m L_3 w t_1(6c_3L_1c_2L_3 + 6c_3L_2L_3 - 6s_3L_1s_2L_3 \\
&\quad +3L_3^2 + w^2 + t_1^2) + 1/12\beta_m L_4 w t_1(12c_3L_1c_2L_3 + \\
&\quad 12c_3L_2L_3 - 12s_3L_1s_2L_3 + 12L_3^2 + 12L_4c_4L_3 + 3L_4^2 \\
&\quad +6L_4c_2c_4c_3L_1 - 6L_4c_2s_4s_3L_1 - 6L_4s_2c_4s_3L_1 - \\
&\quad 6L_4s_2s_4c_3L_1 + 6L_4c_4c_3L_2 - 6L_4s_4s_3L_2 + w^2 + t_1^2)
\end{aligned}
$$

$$
\begin{aligned}
\mathbf{M}_{14} &= 1/12\beta_m L_4 w t_1(3L_4^2 + 6L_4c_4L_3 + 6L_4c_2c_4c_3L_1 - \\
&\quad 6L_4c_2s_4s_3L_1 - 6L_4s_2c_4s_3L_1 - 6L_4s_2s_4c_3L_1 + \\
&\quad 6L_4c_4c_3L_2 - 6L_4s_4s_3L_2 + w^2 + t_1^2)
\end{aligned}
$$

$$
\begin{aligned}
\mathbf{M}_{21} &= 1/12\beta_m L_2 w t_1(6L_1c_2L_2 + 3L_2^2 + w^2 + t_1^2) + \\
&\quad 1/12\beta_m L_3 w t_1(12L_1c_2L_2 + 12L_2^2 + 6c_3L_1c_2L_3 \\
&\quad +12c_3L_2L_3 - 6s_3L_1s_2L_3 + 3L_3^2 + w^2 + t_1^2) + \\
&\quad 1/12\beta_m L_4 w t_1(-12s_3L_1s_2L_3 + 12c_3L_1c_2L_3 + \\
&\quad 12L_1c_2L_2 + t_1^2 + w^2 + 3L_4^2 + 24c_3L_2L_3 + 12L_2^2 \\
&\quad +12L_4c_4L_3 + 6L_4c_2c_4c_3L_1 - 6L_4c_2s_4s_3L_1 - \\
&\quad 6L_4s_2c_4s_3L_1 - 6L_4s_2s_4c_3L_1 + 12L_3^2 + \\
&\quad 12L_4c_4c_3L_2 - 12L_4s_4s_3L_2)
\end{aligned}
$$

$$
\begin{aligned}
\mathbf{M}_{22} &= 1/4L_2^3\beta_m w t_1 + 1/12\beta_m L_2 w^3 t_1 + \\
&\quad 1/12\beta_m L_2 w t_1^3 + 1/12\beta_m L_3 w t_1(12L_2^2 + \\
&\quad 12c_3L_2L_3 + 3L_3^2 + w^2 + t_1^2) + 1/12\beta_m L_4 w t_1 \\
&\quad (24c_3L_2L_3 + 12L_3^2 + 12L_4c_4c_3L_2 + 12L_4c_4L_3 \\
&\quad +3L_4^2 - 12L_4s_4s_3L_2 + 12L_2^2 + w^2 + t_1^2)
\end{aligned}
$$

$$
\begin{aligned}
\mathbf{M}_{23} &= 1/12\beta_m L_3 w t_1(6c_3L_2L_3 + 3L_3^2 + w^2 + t_1^2) + \\
&\quad 1/12\beta_m L_4 w t_1(12c_3L_2L_3 + 12L_3^2 + 6L_4c_4c_3L_2 \\
&\quad +12L_4c_4L_3 + 3L_4^2 - 6L_4s_4s_3L_2 + w^2 + t_1^2)
\end{aligned}
$$

$$
\begin{aligned}
\mathbf{M}_{24} &= 1/12\beta_m L_4 w t_1(6L_4c_4c_3L_2 + 6L_4c_4L_3 + \\
&\quad 3L_4^2 - 6L_4s_4s_3L_2 + w^2 + t_1^2)
\end{aligned}
$$

$$
\begin{aligned}
\mathbf{M}_{31} &= 1/12\beta_m L_3 w t_1 (6c_3 L_1 c_2 L_3 + 6c_3 L_2 L_3 - \\
&\quad 6s_3 L_1 s_2 L_3 + 3L_3^2 + w^2 + t_1^2) + 1/12\beta_m L_4 w t_1 \\
&\quad (12c_3 L_1 c_2 L_3 + 12c_3 L_2 L_3 - 12s_3 L_1 s_2 L_3 \\
&\quad +12L_3^2 + 12L_4 c_4 L_3 + 3L_4^2 + 6L_4 c_2 c_4 c_3 L_1 \\
&\quad -6L_4 c_2 s_4 s_3 L_1 - 6L_4 s_2 c_4 s_3 L_1 - 6L_4 s_2 s_4 c_3 L_1 \\
&\quad +6L_4 c_4 c_3 L_2 - 6L_4 s_4 s_3 L_2 + w^2 + t_1^2)
\end{aligned}
$$

$$
\begin{aligned}
\mathbf{M}_{32} &= 1/12\beta_m L_3 w t_1 (6c_3 L_2 L_3 + 3L_3^2 + \\
&\quad w^2 + t_1^2) + 1/12\beta_m L_4 w t_1 (12c_3 L_2 L_3 \\
&\quad +12L_3^2 + 6L_4 c_4 c_3 L_2 + 12L_4 c_4 \\
&\quad L_3 + 3L_4^2 - 6L_4 s_4 s_3 L_2 + w^2 + t_1^2)
\end{aligned}
$$

$$
\begin{aligned}
\mathbf{M}_{33} &= 1/4L_3^3 \beta_m w t_1 + 1/12\beta_m L_3 w^3 t_1 \\
&\quad +1/12\beta_m L_3 w t_1^3 + 1/12\beta_m L_4 w t_1 \\
&\quad (12L_3^2 + 12L_4 c_4 L_3 + 3L_4^2 + w^2 + t_1^2)
\end{aligned}
$$

$$
\mathbf{M}_{34} = 1/12\beta_m L_4 w t_1 (6L_4 c_4 L_3 + 3L_4^2 + w^2 + t_1^2)
$$

$$\begin{aligned}\mathbf{M}_{41} &= 1/12\beta_m L_4 w t_1 (3L_4^2 + 6L_4 c_4 L_3 + \\ &\quad 6L_4 c_2 c_4 c_3 L_1 - 6L_4 c_2 s_4 s_3 L_1 - \\ &\quad 6L_4 s_2 c_4 s_3 L_1 - 6L_4 s_2 s_4 c_3 L_1 + \\ &\quad 6L_4 c_4 c_3 L_2 - 6L_4 s_4 s_3 L_2 + w^2 + t_1^2)\end{aligned}$$

$$\begin{aligned}\mathbf{M}_{42} &= 1/12\beta_m L_4 w t_1 (6L_4 c_4 c_3 L_2 + 6L_4 c_4 L_3 + \\ &\quad 3L_4^2 - 6L_4 s_4 s_3 L_2 + w^2 + t_1^2)\end{aligned}$$

$$\mathbf{M}_{43} = 1/12\beta_m L_4 w t_1 (6L_4 c_4 L_3 + 3L_4^2 + w^2 + t_1^2)$$

$$\mathbf{M}_{44} = 1/4 L_4^3 \beta_m w t_1 + 1/12\beta_m L_4 w^3 t_1 + 1/12\beta_m L_4 w t_1^3$$

$$
\begin{aligned}
\mathbf{C}_{11} = & (-1/2\beta_m L_2^2 wt_2 L_1 s_2 + 1/24\beta_m L_3 wt_2 \\
& (-24L_1 s_2 L_2 - 12c_3 L_1 s_2 L_3 - 12s_3 L_1 c_2 L_3) \\
& +1/24\beta_m L_4 wt_2(-24L_1 s_2 L_2 - 12L_4 s_2 c_4 c_3 L_1 \\
& +12L_4 s_2 s_4 s_3 L_1 - 12L_4 c_2 c_4 s_3 L_1 - \\
& 12L_4 c_2 s_4 c_3 L_1 - 24c_3 L_1 s_2 L_3 - 24s_3 L_1 c_2 L_3))\dot{\theta}_2 \\
& +(1/24\beta_m L_3 wt_1(-12s_3 L_1 c_2 L_3 - 12s_3 L_2 L_3 - \\
& 12c_3 L_1 s_2 L_3) + 1/24\beta_m L_4 wt_1(-12L_4 c_2 c_4 s_3 L_1 \\
& -12L_4 c_2 s_4 c_3 L_1 - 12L_4 s_2 c_4 c_3 L_1 + \\
& 12L_4 s_2 s_4 s_3 L_1 - 24s_3 L_2 L_3 - 24s_3 L_1 c_2 L_3 \\
& -24c_3 L_1 s_2 L_3 - 12L_4 c_4 s_3 L_2 - 12L_4 s_4 c_3 L_2))\dot{\theta}_3 \\
& +1/24\beta_m L_4 wt_1(-12L_4 s_4 L_3 - 12L_4 c_2 s_4 c_3 L_1 \\
& -12L_4 c_2 c_4 s_3 L_1 + 12L_4 s_2 s_4 s_3 L_1 - \\
& 12L_4 s_2 c_4 c_3 L_1 - 12L_4 s_4 c_3 L_2 - 12L_4 c_4 s_3 L_2)\dot{\theta}_4
\end{aligned}
$$

$$
\begin{aligned}
\mathbf{C}_{12} \;=\; & (-1/2\beta_m L_2^2 wt_1 L_1 s_2 + 1/24\beta_m L_3 wt_1 \\
& (-24L_1 s_2 L_2 - 12c_3 L_1 s_2 L_3 - 12s_3 L_1 c_2 L_3) \\
& +1/24\beta_m L_4 wt_1(-24L_1 s_2 L_2 - 12L_4 s_2 c_4 c_3 L_1 \\
& +12L_4 s_2 s_4 s_3 L_1 - 12L_4 c_2 c_4 s_3 L_1 - \\
& 12L_4 c_2 s_4 c_3 L_1 - 24c_3 L_1 s_2 L_3 - 24s_3 L_1 c_2 L_3))\dot{\theta}_1 \\
& +(-1/2\beta_m L_2^2 wt_1 L_1 s_2 + 1/12\beta_m L_3 wt_1(-12L_1 s_2 L_2 \\
& -6c_3 L_1 s_2 L_3 - 6s_3 L_1 c_2 L_3) + 1/12\beta_m L_4 wt_1 \\
& (-12s_3 L_1 c_2 L_3 - 12c_3 L_1 s_2 L_3 - 12L_1 s_2 L_2 \\
& -6L_4 s_2 c_4 c_3 L_1 + 6L_4 s_2 s_4 s_3 L_1 - 6L_4 c_2 c_4 s_3 L_1 \\
& -6L_4 c_2 s_4 c_3 L_1))\dot{\theta}_2 + (1/24\beta_m L_3 wt_1(-6s_3 L_1 c_2 L_3 \\
& -12s_3 L_2 L_3 - 6c_3 L_1 s_2 L_3) + 1/24\beta_m L_4 wt_1 \\
& (-12c_3 L_1 s_2 L_3 - 12s_3 L_1 c_2 L_3 - 24s_3 L_2 L_3 - \\
& 6L_4 c_2 c_4 s_3 L_1 - 6L_4 c_2 s_4 c_3 L_1 - 6L_4 s_2 c_4 c_3 L_1 \\
& +6L_4 s_2 s_4 s_3 L_1 - 12L_4 c_4 s_3 L_2 - 12L_4 s_4 c_3 L_2) + \\
& 1/24\beta_m L_3 wt_1(-6c_3 L_1 s_2 L_3 - 6s_3 L_1 c_2 L_3) + \\
& 1/24\beta_m L_4 wt_1(-12c_3 L_1 s_2 L_3 - 12s_3 L_1 c_2 L_3 - \\
& 6L_4 s_2 c_4 c_3 L_1 + 6L_4 s_2 s_4 s_3 L_1 - 6L_4 c_2 c_4 s_3 L_1 \\
& -6L_4 c_2 s_4 c_3 L_1))\dot{\theta}_3 + (1/24\beta_m L_4 wt_1 \\
& (-12L_4 s_4 L_3 - 6L_4 c_2 s_4 c_3 L_1 - 6L_4 c_2 c_4 s_3 L_1 + \\
& 6L_4 s_2 s_4 s_3 L_1 - 6L_4 s_2 c_4 c_3 L_1 - 12L_4 s_4 c_3 L_2 - \\
& 12L_4 c_4 s_3 L_2) + 1/24\beta_m L_4 wt_1(-6L_4 s_2 c_4 c_3 L_1 \\
& +6L_4 s_2 s_4 s_3 L_1 - 6L_4 c_2 c_4 s_3 L_1 - 6L_4 c_2 s_4 c_3 L_1))\dot{\theta}_4
\end{aligned}
$$

$$
\begin{aligned}
\mathbf{C}_{13} = {} & (1/24\beta_m L_3 wt_1(-12s_3L_1c_2L_3 - 12s_3L_2L_3 - \\
& 12c_3L_1s_2L_3) + 1/24\beta_m L_4 wt_1(-12L_4c_2c_4s_3L_1 \\
& -12L_4c_2s_4c_3L_1 - 12L_4s_2c_4c_3L_1 + 12L_4s_2s_4s_3L_1 \\
& -24s_3L_2L_3 - 24s_3L_1c_2L_3 - 24c_3L_1s_2L_3 - \\
& 12L_4c_4s_3L_2 - 12L_4s_4c_3L_2))\dot{\theta}_1 + (1/24\beta_m L_3 wt_1 \\
& (-6s_3L_1c_2L_3 - 12s_3L_2L_3 - 6c_3L_1s_2L_3) + \\
& 1/24\beta_m L_4 wt_1(-12c_3L_1s_2L_3 - 12s_3L_1c_2L_3 - \\
& 24s_3L_2L_3 - 6L_4c_2c_4s_3L_1 - 6L_4c_2s_4c_3L_1 - \\
& 6L_4s_2c_4c_3L_1 + 6L_4s_2s_4s_3L_1 - 12L_4c_4s_3L_2 - \\
& 12L_4s_4c_3L_2) + 1/24\beta_m L_3 wt_1(-6c_3L_1s_2L_3 \\
& -6s_3L_1c_2L_3) + 1/24\beta_m L_4 wt_1(-12c_3L_1s_2L_3 - \\
& 12s_3L_1c_2L_3 - 6L_4s_2c_4c_3L_1 + 6L_4s_2s_4s_3L_1 - \\
& 6L_4c_2c_4s_3L_1 - 6L_4c_2s_4c_3L_1))\dot{\theta}_2 + (1/12\beta_m L_3 wt_1 \\
& (-6s_3L_1c_2L_3 - 6s_3L_2L_3 - 6c_3L_1s_2L_3) + \\
& 1/12\beta_m L_4 wt_1(-12s_3L_1c_2L_3 - 12s_3L_2L_3 - \\
& 12c_3L_1s_2L_3 - 6L_4c_2c_4s_3L_1 - 6L_4c_2s_4c_3L_1 \\
& -6L_4s_2c_4c_3L_1 + 6L_4s_2s_4s_3L_1 - 6L_4c_4s_3L_2 - \\
& 6L_4s_4c_3L_2))\dot{\theta}_3 + (1/24\beta_m L_4 wt_1(-12L_4s_4L_3 \\
& -6L_4c_2s_4c_3L_1 - 6L_4c_2c_4s_3L_1 + 6L_4s_2s_4s_3L_1 \\
& -6L_4s_2c_4c_3L_1 - 6L_4s_4c_3L_2 - 6L_4c_4s_3L_2) + \\
& 1/24\beta_m L_4 wt_1(-6L_4c_2c_4s_3L_1 - 6L_4c_2s_4c_3L_1 \\
& -6L_4s_2c_4c_3L_1 + 6L_4s_2s_4s_3L_1 - 6L_4c_4s_3L_2 \\
& -6L_4s_4c_3L_2))\dot{\theta}_4
\end{aligned}
$$

$$
\begin{aligned}
\mathbf{C}_{14} \;=\;& 1/24\beta_m L_4 wt_1(-12L_4 s_4 L_3 - 12L_4 c_2 s_4 c_3 L_1 \\
& -12L_4 c_2 c_4 s_3 L_1 + 12L_4 s_2 s_4 s_3 L_1 - \\
& 12L_4 s_2 c_4 c_3 L_1 - 12L_4 s_4 c_3 L_2 - 12L_4 c_4 s_3 L_2)\dot{\theta}_1 \\
& +(1/24\beta_m L_4 wt_1(-12L_4 s_4 L_3 - 6L_4 c_2 s_4 c_3 L_1 - \\
& 6L_4 c_2 c_4 s_3 L_1 + 6L_4 s_2 s_4 s_3 L_1 - 6L_4 s_2 c_4 c_3 L_1 - \\
& 12L_4 s_4 c_3 L_2 - 12L_4 c_4 s_3 L_2) + 1/24\beta_m L_4 wt_1 \\
& (-6L_4 s_2 c_4 c_3 L_1 + 6L_4 s_2 s_4 s_3 L_1 - 6L_4 c_2 c_4 s_3 L_1 \\
& -6L_4 c_2 s_4 c_3 L_1))\dot{\theta}_2 + (1/24\beta_m L_4 wt_1(-12L_4 s_4 L_3 \\
& -6L_4 c_2 s_4 c_3 L_1 - 6L_4 c_2 c_4 s_3 L_1 + 6L_4 s_2 s_4 s_3 L_1 \\
& -6L_4 s_2 c_4 c_3 L_1 - 6L_4 s_4 c_3 L_2 - 6L_4 c_4 s_3 L_2) + \\
& 1/24\beta_m L_4 wt_1(-6L_4 c_2 c_4 s_3 L_1 - 6L_4 c_2 s_4 c_3 L_1 \\
& -6L_4 s_2 c_4 c_3 L_1 + 6L_4 s_2 s_4 s_3 L_1 - 6L_4 c_4 s_3 L_2 - \\
& 6L_4 s_4 c_3 L_2))\dot{\theta}_3 + 1/12\beta_m L_4 wt_1(-6L_4 s_4 L_3 - \\
& 6L_4 c_2 s_4 c_3 L_1 - 6L_4 c_2 c_4 s_3 L_1 + 6L_4 s_2 s_4 s_3 L_1 - \\
& 6L_4 s_2 c_4 c_3 L_1 - 6L_4 s_4 c_3 L_2 - 6L_4 c_4 s_3 L_2)\dot{\theta}_4
\end{aligned}
$$

$$
\begin{aligned}
\mathbf{C}_{21} \;=\;& (1/2\beta_m L_2^2 wt_1 L_1 s_2 - 1/24\beta_m L_3 wt_1(-24L_1 s_2 L_2 \\
& -12c_3 L_1 s_2 L_3 - 12s_3 L_1 c_2 L_3) - 1/24\beta_m L_4 \\
& wt_1(-24L_1 s_2 L_2 - 12L_4 s_2 c_4 c_3 L_1 + \\
& 12L_4 s_2 s_4 s_3 L_1 - 12L_4 c_2 c_4 s_3 L_1 - 12L_4 c_2 s_4 c_3 L_1 \\
& -24c_3 L_1 s_2 L_3 - 24s_3 L_1 c_2 L_3))\dot{\theta}_1 + (1/24\beta_m L_3 wt_1 \\
& (-6s_3 L_1 c_2 L_3 - 12s_3 L_2 L_3 - 6c_3 L_1 s_2 L_3) + \\
& 1/24\beta_m L_4 wt_1(-12c_3 L_1 s_2 L_3 - 12s_3 L_1 c_2 L_3 - \\
& 24s_3 L_2 L_3 - 6L_4 c_2 c_4 s_3 L_1 - 6L_4 c_2 s_4 c_3 L_1 - \\
& 6L_4 s_2 c_4 c_3 L_1 + 6L_4 s_2 s_4 s_3 L_1 - 12L_4 c_4 s_3 L_2 - \\
& 12L_4 s_4 c_3 L_2) - 1/24\beta_m L_3 wt_1(-6c_3 L_1 s_2 L_3 - \\
& 6s_3 L_1 c_2 L_3) - 1/24\beta_m L_4 wt_1(-12c_3 L_1 s_2 L_3 - \\
& 12s_3 L_1 c_2 L_3 - 6L_4 s_2 c_4 c_3 L_1 + 6L_4 s_2 s_4 s_3 L_1 - \\
& 6L_4 c_2 c_4 s_3 L_1 - 6L_4 c_2 s_4 c_3 L_1))\dot{\theta}_3 + \\
& (1/24\beta_m L_4 wt_1(-12L_4 s_4 L_3 - 6L_4 c_2 s_4 c_3 L_1 - \\
& 6L_4 c_2 c_4 s_3 L_1 + 6L_4 s_2 s_4 s_3 L_1 - 6L_4 s_2 c_4 c_3 L_1 - \\
& 12L_4 s_4 c_3 L_2 - 12L_4 c_4 s_3 L_2) - 1/24\beta_m L_4 wt_1 \\
& (-6L_4 s_2 c_4 c_3 L_1 + 6L_4 s_2 s_4 s_3 L_1 - 6L_4 c_2 c_4 s_3 L_1 \\
& -6L_4 c_2 s_4 c_3 L_1))\dot{\theta}_4
\end{aligned}
$$

$$
\begin{aligned}
\mathbf{C}_{22} \;=\;& (-1/2\beta_m L_3^2 wt_1 s_3 L_2 + 1/24\beta_m L_4 wt_1 \\
& (-24s_3 L_2 L_3 - 12L_4 c_4 s_3 L_2 - 12L_4 s_4 c_3 L_2))\dot{\theta}_3 \\
& +1/24\beta_m L_4 wt_1(-12L_4 s_4 c_3 L_2 - 12L_4 s_4 L_3 - \\
& 12L_4 c_4 s_3 L_2)\dot{\theta}_4
\end{aligned}
$$

$$
\begin{aligned}
\mathbf{C}_{23} = {} & (1/24\beta_m L_3 wt_1(-6s_3 L_1 c_2 L_3 - 12s_3 L_2 L_3 - \\
& 6c_3 L_1 s_2 L_3) + 1/24\beta_m L_4 wt_1(-12c_3 L_1 s_2 L_3 \\
& -12s_3 L_1 c_2 L_3 - 24s_3 L_2 L_3 - 6L_4 c_2 c_4 s_3 L_1 \\
& -6L_4 c_2 s_4 c_3 L_1 - 6L_4 s_2 c_4 c_3 L_1 + 6L_4 s_2 s_4 s_3 L_1 \\
& -12L_4 c_4 s_3 L_2 - 12L_4 s_4 c_3 L_2) - 1/24\beta_m L_3 wt_1 \\
& (-6c_3 L_1 s_2 L_3 - 6s_3 L_1 c_2 L_3) - 1/24\beta_m L_4 wt_1 \\
& (-12c_3 L_1 s_2 L_3 - 12s_3 L_1 c_2 L_3 - 6L_4 s_2 c_4 c_3 L_1 \\
& +6L_4 s_2 s_4 s_3 L_1 - 6L_4 c_2 c_4 s_3 L_1 - 6L_4 c_2 s_4 c_3 L_1)) \\
& \dot{\theta}_1 + (-1/2\beta_m L_3^2 wt_1 s_3 L_2 + 1/24\beta_m L_4 wt_1 \\
& (-24s_3 L_2 L_3 - 12L_4 c_4 s_3 L_2 - 12L_4 s_4 c_3 L_2))\dot{\theta}_2 \\
& +(-1/2\beta_m L_3^2 wt_1 s_3 L_2 + 1/12\beta_m L_4 wt_1 \\
& (-12s_3 L_2 L_3 - 6L_4 c_4 s_3 L_2 - 6L_4 s_4 c_3 L_2))\dot{\theta}_3 \\
& +(1/24\beta_m L_4 wt_1(-6L_4 s_4 c_3 L_2 - 12L_4 s_4 L_3 - \\
& 6L_4 c_4 s_3 L_2) + 1/24\beta_m L_4 wt_1(-6L_4 c_4 s_3 L_2 - \\
& 6L_4 s_4 c_3 L_2))\dot{\theta}_4
\end{aligned}
$$

$$
\begin{aligned}
\mathbf{C}_{24} \;=\; & (1/24\beta_m L_4 wt_1(-12L_4 s_4 L_3 - 6L_4 c_2 s_4 c_3 L_1 \\
& -6L_4 c_2 c_4 s_3 L_1 + 6L_4 s_2 s_4 s_3 L_1 - 6L_4 s_2 c_4 c_3 L_1 \\
& -12L_4 s_4 c_3 L_2 - 12L_4 c_4 s_3 L_2) - 1/24\beta_m L_4 wt_1 \\
& (-6L_4 s_2 c_4 c_3 L_1 + 6L_4 s_2 s_4 s_3 L_1 - 6L_4 c_2 c_4 s_3 L_1 \\
& -6L_4 c_2 s_4 c_3 L_1))\dot{\theta}_1 + 1/24\beta_m L_4 wt_1(-12L_4 s_4 c_3 L_2 \\
& -12L_4 s_4 L_3 - 12L_4 c_4 s_3 L_2)\dot{\theta}_2 + (1/24\beta_m L_4 wt_1 \\
& (-6L_4 s_4 c_3 L_2 - 12L_4 s_4 L_3 - 6L_4 c_4 s_3 L_2) + \\
& 1/24\beta_m L_4 wt_1(-6L_4 c_4 s_3 L_2 - 6L_4 s_4 c_3 L_2))\dot{\theta}_3 + \\
& 1/12\beta_m L_4 wt_1(-6L_4 s_4 c_3 L_2 - 6L_4 s_4 L_3 - 6L_4 c_4 s_3 L_2)\dot{\theta}_4
\end{aligned}
$$

$$
\begin{aligned}
\mathbf{C}_{31} = {} & (-1/24\beta_m L_3 wt_1(-12s_3L_1c_2L_3 - 12s_3L_2L_3 \\
& -12c_3L_1s_2L_3) - 1/24\beta_m L_4 wt_1(-12L_4c_2c_4s_3L_1 \\
& -12L_4c_2s_4c_3L_1 - 12L_4s_2c_4c_3L_1 + 12L_4s_2s_4s_3L_1 \\
& -24s_3L_2L_3 - 24s_3L_1c_2L_3 - 24c_3L_1s_2L_3 - \\
& 12L_4c_4s_3L_2 - 12L_4s_4c_3L_2))\dot{\theta}_1 + (1/24\beta_m L_3 wt_1 \\
& (-6c_3L_1s_2L_3 - 6s_3L_1c_2L_3) + 1/24\beta_m L_4 wt_1 \\
& (-12c_3L_1s_2L_3 - 12s_3L_1c_2L_3 - 6L_4s_2c_4c_3L_1 \\
& +6L_4s_2s_4s_3L_1 - 6L_4c_2c_4s_3L_1 - 6L_4c_2s_4c_3L_1) \\
& -1/24\beta_m L_3 wt_1(-6s_3L_1c_2L_3 - 12s_3L_2L_3 - \\
& 6c_3L_1s_2L_3) - 1/24\beta_m L_4 wt_1(-12c_3L_1s_2L_3 - \\
& 12s_3L_1c_2L_3 - 24s_3L_2L_3 - 6L_4c_2c_4s_3L_1 - \\
& 6L_4c_2s_4c_3L_1 - 6L_4s_2c_4c_3L_1 + 6L_4s_2s_4s_3L_1 - \\
& 12L_4c_4s_3L_2 - 12L_4s_4c_3L_2))\dot{\theta}_2 + (1/24\beta_m L_4 wt_1 \\
& (-12L_4s_4L_3 - 6L_4c_2s_4c_3L_1 - 6L_4c_2c_4s_3L_1 + \\
& 6L_4s_2s_4s_3L_1 - 6L_4s_2c_4c_3L_1 - 6L_4s_4c_3L_2 - \\
& 6L_4c_4s_3L_2) - 1/24\beta_m L_4 wt_1(-6L_4c_2c_4s_3L_1 - \\
& 6L_4c_2s_4c_3L_1 - 6L_4s_2c_4c_3L_1 + 6L_4s_2s_4s_3L_1 - \\
& 6L_4c_4s_3L_2 - 6L_4s_4c_3L_2))\dot{\theta}_4
\end{aligned}
$$

$$
\begin{aligned}
\mathbf{C}_{32} \;=\; & (1/24\beta_m L_3 wt_1(-6c_3L_1s_2L_3 - 6s_3L_1c_2L_3) \\
& +1/24\beta_m L_4 wt_1(-12c_3L_1s_2L_3 - 12s_3L_1c_2L_3 \\
& -6L_4s_2c_4c_3L_1 + 6L_4s_2s_4s_3L_1 - 6L_4c_2c_4s_3L_1 \\
& -6L_4c_2s_4c_3L_1) - 1/24\beta_m L_3 wt_1(-6s_3L_1c_2L_3 \\
& -12s_3L_2L_3 - 6c_3L_1s_2L_3) - 1/24\beta_m L_4 wt_1 \\
& (-12c_3L_1s_2L_3 - 12s_3L_1c_2L_3 - 24s_3L_2L_3 - \\
& 6L_4c_2c_4s_3L_1 - 6L_4c_2s_4c_3L_1 - 6L_4s_2c_4c_3L_1 \\
& +6L_4s_2s_4s_3L_1 - 12L_4c_4s_3L_2 - 12L_4s_4c_3L_2))\dot{\theta}_1 \\
& +(1/2\beta_m L_3^2 wt_1 s_3L_2 - 1/24\beta_m L_4 wt_1(-24s_3L_2L_3 \\
& -12L_4c_4s_3L_2 - 12L_4s_4c_3L_2))\dot{\theta}_2 + (1/24\beta_m L_4 wt_1 \\
& (-6L_4s_4c_3L_2 - 12L_4s_4L_3 - 6L_4c_4s_3L_2) - \\
& 1/24\beta_m L_4 wt_1(-6L_4c_4s_3L_2 - 6L_4s_4c_3L_2))\dot{\theta}_4
\end{aligned}
$$

$$
\mathbf{C}_{33} = -1/2\beta_m L_4^2 wt_1 s_4 L_3 \dot{\theta}_4
$$

$$
\begin{aligned}
\mathbf{C}_{34} = & (1/24\beta_m L_4 wt_1(-12L_4 s_4 L_3 - 6L_4 c_2 s_4 c_3 L_1 \\
& -6L_4 c_2 c_4 s_3 L_1 + 6L_4 s_2 s_4 s_3 L_1 - 6L_4 s_2 c_4 c_3 L_1 \\
& -6L_4 s_4 c_3 L_2 - 6L_4 c_4 s_3 L_2) - 1/24\beta_m L_4 wt_1 \\
& (-6L_4 c_2 c_4 s_3 L_1 - 6L_4 c_2 s_4 c_3 L_1 - 6L_4 s_2 c_4 c_3 L_1 \\
& +6L_4 s_2 s_4 s_3 L_1 - 6L_4 c_4 s_3 L_2 - 6L_4 s_4 c_3 L_2))\dot{\theta}_1 \\
& +(1/24\beta_m L_4 wt_1(-6L_4 s_4 c_3 L_2 - 12L_4 s_4 L_3 - \\
& 6L_4 c_4 s_3 L_2) - 1/24\beta_m L_4 wt_1(-6L_4 c_4 s_3 L_2 - \\
& 6L_4 s_4 c_3 L_2))\dot{\theta}_2 - 1/2\beta_m L_4^2 wt_1 s_4 L_3 \dot{\theta}_3 - \\
& 1/2\beta_m L_4^2 wt_1 s_4 L_3 \dot{\theta}_4
\end{aligned}
$$

$$
\begin{aligned}
\mathbf{C}_{41} = & -1/24\beta_m L_4 wt_1(-12L_4 s_4 L_3 - 12L_4 c_2 s_4 c_3 L_1 \\
& -12L_4 c_2 c_4 s_3 L_1 + 12L_4 s_2 s_4 s_3 L_1 - \\
& 12L_4 s_2 c_4 c_3 L_1 - 12L_4 s_4 c_3 L_2 - 12L_4 c_4 s_3 L_2)\dot{\theta}_1 \\
& +(1/24\beta_m L_4 wt_1(-6L_4 s_2 c_4 c_3 L_1 + 6L_4 s_2 s_4 s_3 L_1 \\
& -6L_4 c_2 c_4 s_3 L_1 - 6L_4 c_2 s_4 c_3 L_1) - 1/24\beta_m L_4 wt_1 \\
& (-12L_4 s_4 L_3 - 6L_4 c_2 s_4 c_3 L_1 - 6L_4 c_2 c_4 s_3 L_1 + \\
& 6L_4 s_2 s_4 s_3 L_1 - 6L_4 s_2 c_4 c_3 L_1 - 12L_4 s_4 c_3 L_2 - \\
& 12L_4 c_4 s_3 L_2))\dot{\theta}_2 + (1/24\beta_m L_4 wt_1(-6L_4 c_2 c_4 s_3 L_1 \\
& -6L_4 c_2 s_4 c_3 L_1 - 6L_4 s_2 c_4 c_3 L_1 + 6L_4 s_2 s_4 s_3 L_1 - \\
& 6L_4 c_4 s_3 L_2 - 6L_4 s_4 c_3 L_2) - 1/24\beta_m L_4 wt_1 \\
& (-12L_4 s_4 L_3 - 6L_4 c_2 s_4 c_3 L_1 - 6L_4 c_2 c_4 s_3 L_1 + \\
& 6L_4 s_2 s_4 s_3 L_1 - 6L_4 s_2 c_4 c_3 L_1 - 6L_4 s_4 c_3 L_2 - \\
& 6L_4 c_4 s_3 L_2))\dot{\theta}_3
\end{aligned}
$$

$$
\begin{aligned}
\mathbf{C}_{42} = {} & (1/24\beta_m L_4 wt_1(-6L_4 s_2 c_4 c_3 L_1 + 6L_4 s_2 s_4 s_3 L_1 \\
& -6L_4 c_2 c_4 s_3 L_1 - 6L_4 c_2 s_4 c_3 L_1) - 1/24\beta_m L_4 wt_1 \\
& (-12L_4 s_4 L_3 - 6L_4 c_2 s_4 c_3 L_1 - 6L_4 c_2 c_4 s_3 L_1 + \\
& 6L_4 s_2 s_4 s_3 L_1 - 6L_4 s_2 c_4 c_3 L_1 - 12L_4 s_4 c_3 L_2 - \\
& 12L_4 c_4 s_3 L_2))\dot{\theta}_1 - 1/24\beta_m L_4 wt_1(-12L_4 s_4 c_3 L_2 \\
& -12L_4 s_4 L_3 - 12L_4 c_4 s_3 L_2)\dot{\theta}_2 + (1/24\beta_m L_4 wt_1 \\
& (-6L_4 c_4 s_3 L_2 - 6L_4 s_4 c_3 L_2) - 1/24\beta_m L_4 wt_1 \\
& (-6L_4 s_4 c_3 L_2 - 12L_4 s_4 L_3 - 6L_4 c_4 s_3 L_2))\dot{\theta}_3
\end{aligned}
$$

$$
\begin{aligned}
\mathbf{C}_{43} = {} & (1/24\beta_m L_4 wt_1(-6L_4 c_2 c_4 s_3 L_1 - 6L_4 c_2 s_4 c_3 L_1 \\
& -6L_4 s_2 c_4 c_3 L_1 + 6L_4 s_2 s_4 s_3 L_1 - 6L_4 c_4 s_3 L_2 \\
& -6L_4 s_4 c_3 L_2) - 1/24\beta_m L_4 wt_1(-12L_4 s_4 L_3 - \\
& 6L_4 c_2 s_4 c_3 L_1 - 6L_4 c_2 c_4 s_3 L_1 + 6L_4 s_2 s_4 s_3 L_1 \\
& -6L_4 s_2 c_4 c_3 L_1 - 6L_4 s_4 c_3 L_2 - 6L_4 c_4 s_3 L_2))\dot{\theta}_1 \\
& +(1/24\beta_m L_4 wt_1(-6L_4 c_4 s_3 L_2 - 6L_4 s_4 c_3 L_2) \\
& -1/24\beta_m L_4 wt_1(-6L_4 s_4 c_3 L_2 - 12L_4 s_4 L_3 \\
& -6L_4 c_4 s_3 L_2))\dot{\theta}_2 + 1/2\beta_m L_4^2 wt_1 s_4 L_3 \dot{\theta}_3
\end{aligned}
$$

$$
\mathbf{C}_{44} = 0
$$

Part II

Appendix B: Geometric and Material Parameters for Corner Cube

The following parameters describe the corner cube geometry. The remaining material properties are equivalent to those defined in Appendix A.

Parameter	Value	Units
l	64	μm
l^c	71	μm
L	300	μm

Table 3. Parameters for corner cube

The following represent the Jacobians, mass, and Coriolis matrices for the reduced open chain system, respectively:

$$\mathbf{J}_1 = \begin{bmatrix} 0 & 0 & 0 \\ 0 & 0 & 0 \\ 0.778L & 0 & 0 \\ -1 & 0 & 0 \\ -1 & 0 & 0 \\ 0 & 0 & 0 \end{bmatrix}$$

$$\mathbf{J}_2 = \begin{bmatrix} -1/2s_2L & 0 & 0 \\ 1/2s_2L & 0 & 0 \\ 1/2(-1+c_2)L & 1/2L & 0 \\ -1 & 1 & 0 \\ -c_2 & 0 & 0 \\ s_2 & 0 & 0 \end{bmatrix}$$

$$\mathbf{J}_3 = \begin{bmatrix} 1/2(s_3 - s_2c_3)L & -1/2s_3L & 0 \\ 1/2(s_3 - s_2c_3)L & -1/2s_3L & 0 \\ -1/2(c_2 + s_3s_2 + c_3)L & 1/2Lc_3 & 1/2L \\ -s_3s_2 - c_3 & c_3 & 0 \\ -c_2 & 0 & 1 \\ -s_3 + s_2c_3 & s_3 & 0 \end{bmatrix}$$

$$
\begin{aligned}
\mathbf{M}_{11} &= 0.33\beta_m L\hat{}4t_1 + 2\beta_m(1/24L^2t_1^3 + 1/36L\hat{}4t_1) \\
&\quad +2/3s_2^2L\hat{}4\beta_m t_1 + 1/4(-1+c_2)^2L\hat{}4\beta_m t_1 + \\
&\quad 1/12\beta_m L^2t_1(L^2+t_1^2) + 1/12c_2^2\beta_m L^2t_1(L^2+t_1^2) \\
&\quad +1/12\beta_m L^2t_1(12L^2 - 8L^2s_3s_2c_3 - 4L^2c_3^2c_2^2 + \\
&\quad 6L^2c_2s_3s_2 + 6L^2c_2c_3 + t_1^2 + t_1^2c_2^2c_3^2 + 2s_3s_2c_3t_1^2)
\end{aligned}
$$

$$
\begin{aligned}
\mathbf{M}_{12} &= 1/4(-1+c_2)L\hat{}4\beta_m t_1 - 1/12\beta_m L^2t_1(L^2+t_1^2) \\
&\quad -1/12\beta_m L^2t_1(8L^2 - 4L^2c_3^2 - 4L^2s_3s_2c_3 + \\
&\quad 3L^2c_2c_3 + s_3s_2c_3t_1^2 + c_3^2t_1^2)
\end{aligned}
$$

$$
\mathbf{M}_{13} = -1/12\beta_m L^2t_1(4L^2c_2 + 3s_3s_2L^2 + 3L^2c_3 + c_2t_1^2)
$$

$$
\begin{aligned}
\mathbf{M}_{21} &= 1/4(-1+c_2)L\hat{}4\beta_m t_1 - 1/12\beta_m L^2t_1(L^2+t_1^2) \\
&\quad -1/12\beta_m L^2t_1(8L^2 - 4L^2c_3^2 - 4L^2s_3s_2c_3 + \\
&\quad 3L^2c_2c_3 + s_3s_2c_3t_1^2 + c_3^2t_1^2)
\end{aligned}
$$

$$
\begin{aligned}
\mathbf{M}_{22} &= 1/4\beta_m L\hat{}4t_1 + 1/12\beta_m L^2t_1(L^2+t_1^2) + \\
&\quad 1/12\beta_m L^2t_1(8L^2 - 4L^2c_3^2 + c_3^2t_1^2)
\end{aligned}
$$

$$
\mathbf{M}_{23} = 1/4L\hat{}4c_3\beta_m t_1
$$

$$\mathbf{M}_{31} = -1/12\beta_m L^2 t_1(4L^2 c_2 + 3s_3 s_2 L^2 + 3L^2 c_3 + c_2 t_1^2)$$

$$\mathbf{M}_{32} = 1/4L\hat{}4c_3\beta_m t_1$$

$$\mathbf{M}_{33} = 1/3\beta_m L\hat{}4t_1 + 1/12\beta_m L^2 t_1^3$$

$$\begin{aligned}
\mathbf{C}_{11} \;=\; & (2/3s_2 L\hat{}4\beta_m t_1 c_2 - 1/4(-1+c_2)L\hat{}4\beta_m t_1 s_2 \\
& -1/12c_2\beta_m L^2 t_1(L^2 + t_1^2)s_2 + 1/24\beta_m L^2 t_1 \\
& (-8L^2 s_3 c_2 c_3 + 8L^2 c_3^2 c_2 s_2 - 6L^2 s_2^2 s_3 + 6L^2 c_2^2 s_3 \\
& -6L^2 s_2 c_3 - 2t_1^2 c_2 c_3^2 s_2 + 2s_3 c_2 c_3 t_1^2))\dot{\theta}_2 + \\
& 1/24\beta_m L^2 t_1(-8L^2 c_3^2 s_2 + 8L^2 s_3^2 s_2 + 8L^2 c_3 c_2^2 s_3 \\
& +6L^2 c_2 c_3 s_2 - 6L^2 c_2 s_3 - 2t_1^2 c_2^2 c_3 s_3 + \\
& 2c_3^2 s_2 t_1^2 - 2s_3^2 s_2 t_1^2)\dot{\theta}_3
\end{aligned}$$

$$\begin{aligned}
\mathbf{C}_{12} \;=\; & (2/3s_2 L\hat{}4\beta_m t_1 c_2 - 1/4(-1+c_2)L\hat{}4\beta_m t_1 s_2 \\
& -1/12c_2\beta_m L^2 t_1(L^2 + t_1^2)s_2 + 1/24\beta_m L^2 t_1 \\
& (-8L^2 s_3 c_2 c_3 + 8L^2 c_3^2 c_2 s_2 - 6L^2 s_2^2 s_3 + 6L^2 c_2^2 s_3 \\
& -6L^2 s_2 c_3 - 2t_1^2 c_2 c_3^2 s_2 + 2s_3 c_2 c_3 t_1^2))\dot{\theta}_1 + \\
& (-1/4s_2 L\hat{}4\beta_m t_1 - 1/12\beta_m L^2 t_1(-4L^2 s_3 c_2 c_3 - \\
& 3L^2 s_2 c_3 + s_3 c_2 c_3 t_1^2))\dot{\theta}_2 + (-1/24\beta_m L^2 t_1(8L^2 c_3 s_3 \\
& -4L^2 c_3^2 s_2 + 4L^2 s_3^2 s_2 - 3L^2 c_2 s_3 + c_3^2 s_2 t_1^2 - \\
& s_3^2 s_2 t_1^2 - 2c_3 t_1^2 s_3) - 1/24\beta_m L^2 t_1(-4L^2 s_2 + \\
& 3L^2 c_2 s_3 - s_2 t_1^2))\dot{\theta}_3
\end{aligned}$$

$$
\begin{aligned}
\mathbf{C}_{13} &= 1/24\beta_m L^2 t_1(-8L^2c_3^2s_2 + 8L^2s_3^2s_2 + 8L^2c_3c_2^2s_3 \\
&\quad +6L^2c_2c_3s_2 - 6L^2c_2s_3 - 2t_1^2c_2^2c_3s_3 + 2c_3^2s_2t_1^2 \\
&\quad -2s_3^2s_2t_1^2)\dot{\theta}_1 + (-1/24\beta_m L^2 t_1(8L^2c_3s_3 - \\
&\quad 4L^2c_3^2s_2 + 4L^2s_3^2s_2 - 3L^2c_2s_3 + c_3^2s_2t_1^2 - s_3^2s_2t_1^2 \\
&\quad -2c_3t_1^2s_3) - 1/24\beta_m L^2 t_1(-4L^2s_2 + 3L^2c_2s_3 \\
&\quad -s_2t_1^2))\dot{\theta}_2 - 1/12\beta_m L^2 t_1(3L^2s_2c_3 - 3L^2s_3)\dot{\theta}_3
\end{aligned}
$$

$$
\begin{aligned}
\mathbf{C}_{21} &= (-2/3s_2L\hat{}4\beta_m t_1c_2 + 1/4(-1+c_2)L\hat{}4\beta_m t_1s_2 \\
&\quad +1/12c_2\beta_m L^2 t_1(L^2+t_1^2)s_2 - 1/24\beta_m L^2 t_1 \\
&\quad (-8L^2s_3c_2c_3 + 8L^2c_3^2c_2s_2 - 6L^2s_2^2s_3 + \\
&\quad 6L^2c_2^2s_3 - 6L^2s_2c_3 - 2t_1^2c_2c_3^2s_2 + 2s_3c_2c_3t_1^2))\dot{\theta}_1 \\
&\quad +(-1/24\beta_m L^2 t_1(8L^2c_3s_3 - 4L^2c_3^2s_2 + 4L^2s_3^2s_2 \\
&\quad -3L^2c_2s_3 + c_3^2s_2t_1^2 - s_3^2s_2t_1^2 - 2c_3t_1^2s_3) + \\
&\quad 1/24\beta_m L^2 t_1(-4L^2s_2 + 3L^2c_2s_3 - s_2t_1^2))\dot{\theta}_3
\end{aligned}
$$

$$
\mathbf{C}_{22} = 1/24\beta_m L^2 t_1(8L^2c_3s_3 - 2c_3t_1^2s_3)\dot{\theta}_3
$$

$$
\begin{aligned}
\mathbf{C}_{23} &= (-1/24\beta_m L^2 t_1(8L^2c_3s_3 - 4L^2c_3^2s_2 \\
&\quad +4L^2s_3^2s_2 - 3L^2c_2s_3 + c_3^2s_2t_1^2 - s_3^2s_2t_1^2 \\
&\quad -2c_3t_1^2s_3) + 1/24\beta_m L^2 t_1(-4L^2s_2 + \\
&\quad 3L^2c_2s_3 - s_2t_1^2))\dot{\theta}_1 + 1/24\beta_m L^2 t_1 \\
&\quad (8L^2c_3s_3 - 2c_3t_1^2s_3)\dot{\theta}_2 - 1/4L\hat{}4s_3\beta_m t_1\dot{\theta}_3
\end{aligned}
$$

$$
\begin{aligned}
\mathbf{C}_{31} = & -1/24\beta_m L^2 t_1(-8L^2 c_3^2 s_2 + 8L^2 s_3^2 s_2 + \\
& 8L^2 c_3 c_2^2 s_3 + 6L^2 c_2 c_3 s_2 - 6L^2 c_2 s_3 \\
& -2t_1^2 c_2^2 c_3 s_3 + 2c_3^2 s_2 t_1^2 - 2s_3^2 s_2 t_1^2)\dot{\theta}_1 + \\
& (-1/24\beta_m L^2 t_1(-4L^2 s_2 + 3L^2 c_2 s_3 - \\
& s_2 t_1^2) + 1/24\beta_m L^2 t_1(8L^2 c_3 s_3 - 4L^2 c_3^2 s_2 \\
& +4L^2 s_3^2 s_2 - 3L^2 c_2 s_3 + c_3^2 s_2 t_1^2 - s_3^2 s_2 t_1^2 \\
& -2c_3 t_1^2 s_3))\dot{\theta}_2
\end{aligned}
$$

$$
\begin{aligned}
\mathbf{C}_{32} = & (-1/24\beta_m L^2 t_1(-4L^2 s_2 + 3L^2 c_2 s_3 \\
& -s_2 t_1^2) + 1/24\beta_m L^2 t_1(8L^2 c_3 s_3 - 4L^2 c_3^2 s_2 \\
& +4L^2 s_3^2 s_2 - 3L^2 c_2 s_3 + c_3^2 s_2 t_1^2 - s_3^2 s_2 t_1^2 \\
& -2c_3 t_1^2 s_3))\dot{\theta}_1 - 1/24\beta_m L^2 t_1(8L^2 c_3 s_3 \\
& -2c_3 t_1^2 s_3)\dot{\theta}_2
\end{aligned}
$$

$$
\mathbf{C}_{33} = 0
$$

Bibliography

[1] S.M. Jurga, "3D micro and nanomanufacturing via folding of 2D membranes," M.S. Thesis. In *Dept. of Mechanical Engineering.* Cambridge, MA: Massachusetts Institute of Technology, 2003, pp. 16-42, 77-96.

[2] J.T. Hastings, F. Zhang, and H.I. Smith, "Nanometer-level stitching in raster-scanning electron-beam lithography using spatial-phase locking," *Journal of Vacuum Science & Technology B*, vol. 21, pp. 2650-2656, 2003.

[3] M. Qi, E. Lidorikis, P. T. Rakich, S. G. Johnson, J. D. Joannopoulos, E. P. Ippen and H. I. Smith, "A three-dimensional optical photonic crystal with designed point defects," *Nature*, vol. 429, pp. 538-542, 2004.

[4] M.C. Purdy. (2005, September 2.2). Atlas of the folds of the cerebral cortex. *Medical News Today* [Online]. Available: http://www.medicalnewstoday.com/medicalnews.php?newsid=30973.

[5] C. Ho and M. Madrid (2005). Looking for a blood substitute. Pittsburgh Supercomputing Center Website [Online]. Available: http://www.psc.edu/science/Ho/Ho.html#hemoglobin.

[6] N. Amato and G. Song, "Using Motion Planning to Study Protein Folding Pathways," *Journal of Computational Biology,* vol. 9, no. 2, pp. 149-168, April 2002.

[7] H.J. In, S. Kumar, Y. Shao-Horn, and G. Barbastathis, "Origami Fabrication of Nanostructured 3D Devices: Electrochemical Capacitor with Carbon Electrodes," *Applied Physics Letters,* to appear.

[8] J.B. Pendry, "A Chiral Route to Negative Refraction," *Science,* vol. 306, no. 5700, pp. 1353-1355, 19 November 2004.

[9] M.C.K. Wiltshire, J.V. Hajnal, J.B. Pendry, D.J. Edwards, and C.J. Stevens, "Metamaterial endoscope for magnetic field transfer: Near field imaging with magnetic wires," *Optics Express,* vol. 11, no. 7, April 2003, pp. 709-715.

[10] J. Cybulski, "Modeling and Fabrication of Self-Assembling Micron-Scale Rollup Structures," M.S. Thesis. In *Dept. of Mechanical Engineering.* Cambridge, MA: Massachusetts Institute of Technology, 2004.

[11] W. Arora, A. Nichol, H.I. Smith, and G. Barbastathis, "Membrane folding to achieve three-dimensional nanostructures: nanopatterned silicon nitride folded with stressed chromium hinges," *Applied Physics Letters*, to appear.

[12] I. Streinu, "Pseudotriangulations, rigidity, and motion planning," *Discrete and Computational Geometry*, vol. 34, no. 4, pp. 587-635, Dec. 2005.

[13] R. Connelly, E.D. Demaine, and G. Rote, "Straightening polygonal arcs and convexifying polygonal cycles." In *Proceedings of the 41st Annual Symposium on Foundations of Computer Science (FOCS 2000)*, Redondo Beach, California, November 12-14, 2000, pp. 432-442.

[14] R. Connelly, E.D. Demaine, and G. Rote, "Straightening polygonal arcs and convexifying polygonal cycles." *Discrete and Comp. Geometry*, 30 (2): 205-239, September 2003.

[15] J.H. Cantarella, E.D. Demaine, H.N. Iben, and J.F. O'Brien, "An energy-driven approach to linkage unfolding." In *Proceedings of the 20th Annual ACM Symposium on Computational Geometry*, Brooklyn, NY, June 2004.

[16] I. Streinu, "A combinatorial approach to planar non-colliding robot arm motion planning." In *Proc. 41st Annual IEEE Sympos. Found. Comput. Sci. IEEE*, November 2000. pp. 443-453.

[17] E.D. Demaine, "Folding and Unfolding." Ph.D. Thesis. In *Dept. of Computer Science.* University of Waterloo, Canada, 2001.

[18] E.D. Demaine and J. O'Rourke. *Geometric Folding Algorithms: Linkages, Origami, and Polyhedra.* Book in preparation, Cambridge University Press.

[19] E.D. Demaine, M.L. Demaine, and J.S.B. Mitchell, "Folding flat silhouettes and wrapping polyhedral packages: new results in computational origami," *Comput. Geom. Theory Appl.*, 16 (1):3-21, 2000.

[20] I. Streinu and W. Whiteley, "Single-vertex origami and 3-dimensional expansive motions." In *Proc. Japan Conf. Discrete and Comp. Geometry*, Tokai University, Tokyo, Japan, Oct. 8-11, 2004.

[21] s.m. belcastro and T. Hull, " Modeling the folding of paper into three dimensions using affine transformations," *Linear Algebra and its Applications*, vol. 348, pp. 273-282, 2002.

[22] T. Buchner, "Kinematics of 3D Folding Structures for Nanostructured Origami," Diploma Thesis, Laboratory for Machine Tools and Production Engineering, RWTH Aachen University (2004), URL: web.mit.edu/optics/www/publications/.

[23] R.M Murray, Z. Li, and S.S. Sastry, *A Mathematical Introduction to Robotic Manipulation.* Boca Raton, FL: CRC Press, 1994, Ch. 2-5.

[24] R.P. Paul, *Robot Manipulators: Mathematics, Programming, and Control.* Cambridge, MA: Massachusetts Institute of Technology, 1981.

[25] H. Asada and J.J. Slotine, *Robot analysis and control,* New York: Wiley, 1986.

[26] J. Wittenburg, *Dynamics of Systems of Rigid Bodies.* Stuttgart: B.G. Teubner, 1977.

[27] J.Y.S. Luh and Y. Zheng, "Computation of Input Generalized Forces for Robots with Closed Kinematic Chain Mechanisms," *IEEE J. Robotics Automat.*, vol. RA-1, no. 2, pp. 95-103, June 1985.

[28] J.J. Murray and G.H. Lovell, "Dynamic modeling of closed-chain manipulators and implications for trajectory control," *IEEE Transactions on Robotics and Automation*, vol. 3, no. 4, pp. 522-528, August 1989.

[29] Y. Nakamura and M. Ghodoussi, "A computational scheme of closed link robot dynamics derived by D'Alembert Principle," In *Proc. 1988 IEEE Int. Conf. on Robotics and Automation,* Philadelphia, PA, Apr. 24-29, 1988, pp. 1354-1360.

[30] H. Baruh, *Analytical Dynamics.* McGraw-Hill, 1999, p. 253-302.

[31] J.R. Barber, *Intermediate Mechanics of Materials.* New York: McGraw-hill, 2001, p. 107.

[32] Nielson, G.N., Seneviratne, D., Lopez-Royo, F., Rakich, P.T., Avrahami, Y., Watts, M.R., Haus, H.A., Tuller, H.L., and Barbastathis, G. "Integrated wavelength-selective optical MEMS switching using ring resonator filters," *IEEE Photonics Technology Letters,* vol. 17, no. 6, pp. 1190-1192, June 2005.

[33] N. Razmara, D. Kohli, and A.K. Dhingra, "On the degrees of freedom of motion of planar-spatial mechanisms," In *Proc. ASME 2000 Design Engineering Technical Conferences and Computer and Information in Engineering Conference*, Baltimore, MD, Sept. 16-17, 2000.